Copyright Warning & Restrictions

The copyright law of the United States (Title 17, United States Code) governs the making of photocopies or other reproductions of copyrighted material.

Under certain conditions specified in the law, libraries and archives are authorized to furnish a photocopy or other reproduction. One of these specified conditions is that the photocopy or reproduction is not to be "used for any purpose other than private study, scholarship, or research." If a, user makes a request for, or later uses, a photocopy or reproduction for purposes in excess of "fair use" that user may be liable for copyright infringement,

This institution reserves the right to refuse to accept a copying order if, in its judgment, fulfillment of the order would involve violation of copyright law.

Please Note: The author retains the copyright while the New Jersey Institute of Technology reserves the right to distribute this thesis or dissertation

Printing note: If you do not wish to print this page, then select "Pages from: first page # to: last page #" on the print dialog screen

ABSTRACT

DISPERSION OF PARTICLES ON LIQUID SURFACES

by

Sathishkumar Gurupatham

When small particles (e.g., flour, pollen, etc.) come in contact with a liquid surface, they immediately disperse. The dispersion can occur so quickly that it appears explosive, especially for small particles on the surface of mobile liquids like water. This explosive dispersion is the consequence of capillary force pulling particles into the interface causing them to accelerate to a relatively large velocity. The maximum velocity increases with decreasing particle size; for nanometer-sized particles (e.g., viruses and proteins), the velocity on an air-water interface can be as large as 47 m/s. They also oscillate at a relatively high frequency about their floating equilibrium before coming to stop under viscous drag. The observed dispersion is a result of strong repulsive hydrodynamic forces that arise because of these oscillations. Experiments were conducted to validate the Direct Numerical Simulation results which were available already.

This dispersion of particles was also witnessed on the liquid-liquid interface. The dispersion on a liquid-liquid interface was relatively weaker than on an air-liquid interface, and occurred over a longer period of time. This was a consequence of the fact that particles became separated while sedimenting through the upper liquid and reached the interface over a time interval that lasted for several seconds. The rate of dispersion depended on the size of particles, the particle and liquids densities, the viscosities of the

liquids involved, and the contact angle. The frequency of oscillation of particles about their floating equilibrium increased with decreasing particle size on both air-water and liquid-liquid interfaces, and the time taken to reach equilibrium decreased with decreasing particle size. These results are in agreement with the analysis.

Although it is known that a clump of powder floating on a liquid surface breaks up to form a particle monolayer on the surface, the mechanism that causes this break up remains abstruse. It is shown that a floating clump breaks up because when particles on its outer periphery of a floating clump come into contact with the liquid surface they are pulled into the interface by the vertical component of capillary force overcoming the cohesive forces which keep them attached and move away from the clump. The latter is a consequence of the fact that when a particle is adsorbed on to a liquid surface it causes a flow away from itself on the interface. This flow causes the newly-adsorbed particles to move away from the clump, and thus the clump size decreases with time and this exposes a new layer of particles that are then adsorbed onto the liquid surface. Interestingly, when many particles are asymmetrically broken apart from a clump's periphery the clump itself is pushed away in the opposite direction by the newly adsorbed particles.

DISPERSION OF PARTICLES ON LIQUID SURFACES

by
Sathishkumar Gurupatham

A Dissertation
Submitted to the Faculty of
New Jersey Institute of Technology
in Partial Fulfillment of the Requirements for the Degree of
Doctor of Philosophy in Mechanical Engineering

Department of Mechanical Engineering

May 2011

APPROVAL PAGE

DISPERSION OF PARTICLES ON LIQUID SURFACES

Sathishkumar Gurupatham

Dr. Pushpendra Singh, Dissertation Co-Advisor — Date
Professor of Mechanical and Industrial Engineering, NJIT

Dr. Ian S. Fischer, Dissertation Co-Advisor — Date
Professor of Mechanical and Industrial Engineering, NJIT

Dr. Anthony D. Rosato, Committee Member — Date
Professor of Mechanical and Industrial Engineering, NJIT

Dr. I Joga Rao, Committee Member — Date
Associate Professor of Mechanical and Industrial Engineering, NJIT

Dr. Denis L. Blackmore, Committee Member — Date
Professor of Mathematical Sciences, NJIT

BIOGRAPHICAL SKETCH

Author: Sathishkumar Gurupatham

Degree: Doctor of Philosophy

Date: May 2011

Undergraduate and Graduate Education:

- Doctor of Philosophy in Mechanical Engineering,
  New Jersey Institute of Technology, Newark, NJ, 2011
- Bachelor of Science in Mechanical Engineering,
  Thanthai Periyar Government Institute of Technology, India, 1993

Major: Mechanical Engineering

Journal Publications:

Pushpendra Singh, Daniel D. Joseph, Sathish K. Gurupatham, Bhavin Dalal, and Sai Nudurupati, Spontaneous dispersion of particles on liquid surfaces, PNAS, 0910343106 (2009).

Sathish K Gurupatham, B. Dalal, M. Hossain, I.S. Fischer, P. Singh, D.D. Joseph, Dispersion of Particles on Fluid-Liquid Interfaces, to appear in Particuology.

Sathish K Gurupatham , M.Hossain, I.S. Fischer, P. Singh, D.D. Joseph, Spreading of solid powder particles over liquid surfaces, submitted to Powder Techonlogy.

Pushpendra Singh, Sathish K. Gurupatham, Bhavin Dalal, Improving the shear strength of the rheological liquid using external electric fields, in preparation.

B. Dalal, S. Gurupatham, J. Cuadra, P. Singh, A. D. Rosato, I. Fischer, Forced oscillation of a particle on a fluid-liquid interface, in preparation.

Conference Publications:

Sathish K. Gurupatham, Bhavin Dalal, Sai Nudurupati, Ian Fischer, Pushpendra Singh, Daniel D. Joseph, Spontaneous dispersion of particles on Air water interface, Seventh Annual Conference on Frontiers in Applied and Computational Mathematics(FACM) on May 21-May 23, 2010

Sathish K. Gurupatham Bhavin Dalal, Sai Nudurupati, Ian Fischer, Pushpendra Singh, Daniel D. Joseph, Spontaneous dispersion of particles on liquid surfaces, 16th US National Congress on Theoretical and Applied Mechanics (USNCTAM) on June 27 - July 2, 2010.

Sathish K. Gurupatham, B. Dalal, M. Hossain, I.S. Fischer, P. Singh, D.D. Joseph, Dispersion of Particles on Fluid-Liquid Interfaces, ASME 2010 Fluids Engineering Summer Meeting (FEDSM2010) on August 1-5, 2010

Sathish K. Gurupatham, M. Hossain, I.S. Fischer, P. Singh, D.D. Joseph, Break up of particle clumps on liquid surfaces, 63rd Annual Meeting of the APS Division of Fluid Dynamics on November 21-23, 2010

TO

My Parents, Wife and lovely Daughter

ACKNOWLEDGMENT

First and foremost, I would first like to thank Lord, Sri Venkateshwara who has been guiding me through the ups and downs of my life. I would thank my parents wholeheartedly for being very supportive and instrumental to see me do my higher education. Their blessing and love is divine and they have exemplified good morals which I appreciate and try to follow their foot prints in my life path. I also express my gratitude to my beloved wife who has been always part of my pleasure and sorrow and motivates me by taking care of the family leaving me free so as to concentrate more on my studies and reminds me of my responsibilities in my day to day activities. It is worth to acknowledge my daughter's support and sacrifice which is unbelievable for her small age. I also extend my thanks to my siblings and my wife's family members for their continued encouragement.

I would now like to thank the foremost person Dr. Pushpendra Singh who shaped me up to become a better researcher. His excellent guidance and incessant encouragement have made me a different person who has realized the significance and inevitability of being a hard worker to succeed in this competitive time. He is very much down-to-earth to understand students' problems and advises simple solutions for the complicated problems which is his unique style made my research work simple and relishable. He is very professional at the work and at the same time very affable and takes utmost care of the students personally.

I thank heartfully Dr. Fischer for his love, care and guidance which have helped me a lot. I also extend my thanks to Dr. Rosato, Dr. Blackmore, Dr. I J Rao, Dr. Behi Mohammad for their interest and support in my research.

My friends also have contributed greatly to complete my research successfully and made me enjoy my stay at NJIT. I am especially thankful to Dr. Sai and Dr. Mansoor who have helped me not only in my research but also consoled and encouraged during my blues. I also thank my current group members Bhavin and Shahadat for their contribution in my research and friendship. I am grateful to Jaskirat for all his help and support as a friend.

Last but not the least would be thanking all people who have helped me directly or indirectly in completing my work. This research was supported by National Science Foundation, the New Jersey Commission on Science and Technology through the New Jersey Center for Micro-Flow Control.

TABLE OF CONTENTS

TABLE OF CONTENTS
(Continued)

Chapter **Page**

LIST OF FIGURES

LIST OF FIGURES

(Continued)

LIST OF FIGURES
(Continued)

LIST OF FIGURES
(Continued)

CHAPTER 1

INTRODUCTION

In recent years, significant effort has been made to understand the behavior of particles trapped at fluid–liquid interfaces because of its importance in a wide range of applications and physical problems, e.g., the self-assembly of particles at fluid–fluid interfaces, the stabilization of emulsions, the pollination in hydrophilous plants, the flotation of insect eggs, the dispersion of viruses and protein macromolecules, etc [1-7].

The following experiment is not only exciting to do but also can be easily performed in any reasonably well-equipped kitchen. If a dish is partially filled with water and after the water became quiescent, a small amount of wheat or corn flour is sprinkled onto the water surface, the moment the flour comes in contact with the surface it quickly disperses into an approximately circular shaped region, forming a monolayer of dispersed flour particles on the surface (Figure 1.1). The interfacial forces that cause this sudden dispersion of flour particles are, in fact, so strong that a few milligrams of flour sprinkled onto the surface almost instantaneously covers the entire surface of the water contained in the dish. The above experiment can be performed using other finely granulated powders (e.g., corn flour, salt, sugar, sand, etc.) or even small seeds, such as mustard and sesame seeds and pollen (Figure 1.2). The tendency of powders to disperse, however, varies. The fact that salt and sugar dissolve in water is not important in this experiment, because the dispersion occurs at a time scale that is much smaller than the time taken by particles to dissolve. Also, the speed with which particles dispersed increases with decreasing their size.

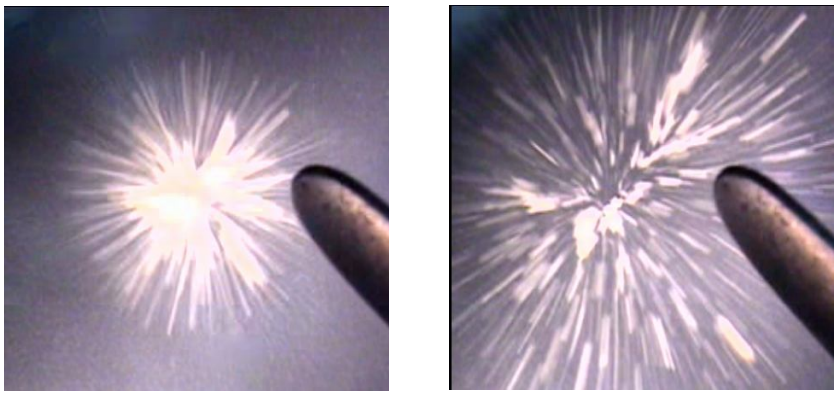

t = 0.033 s t = 0.067 s

Figure 1.1 Wheat flour particles of 2-100 micron size at two time intervals on water surface.

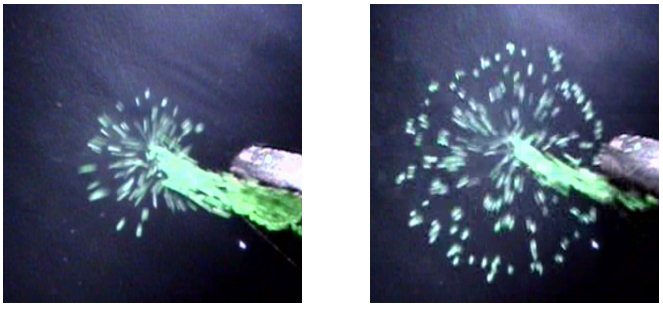

t = 0.033 s t = 0.181 s

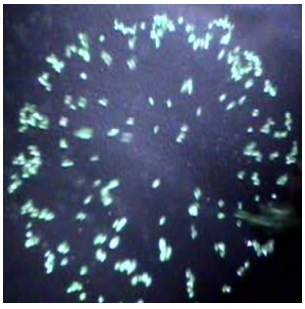

t = 0.363 s

Figure 1.2 Colored Sand particles of 200 micron size at various time intervals on water surface.

Above all, the newly adsorbed particles cause particles already adsorbed on the interface to move away, too. The Figure.1.3 shows that a newly adsorbed particle creates a

circular particle-free region around itself, the radius of which can be several times larger than its own radius.

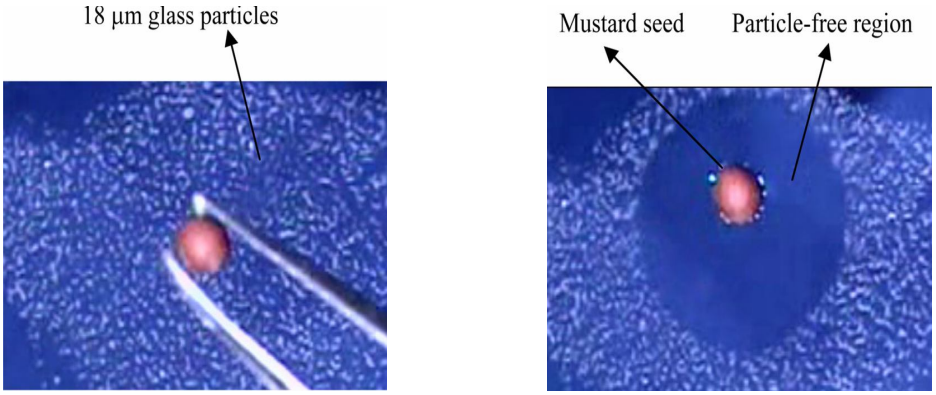

Figure 1.3 Dispersion of particles trapped on the surface due to a newly adsorbed particle. (Left) A mustard seed of diameter 1.1mm being dropped onto a monolayer of 18μm glass particles on the surface of a 60% glycerin in water. (Right) The mustard seed causes all of the nearby glass particles to move away, and thus creates an approximately circular particle-free region.

The aim of this research was to study the fluid dynamics of initial explosive dispersion of particles on air-liquid interface as well as liquid-liquid interface and relate it to the real time phenomena like the breakup of a clump of particles when it is placed on a liquid surface so as to unravel the mysteries of dynamics behind them.

1.1 Literature Review

Though small particles first dispersed violently at large speeds, later they slowly came back to form monolayer clusters due to attractive lateral capillary forces. The same dynamics were observed for more viscous liquids except that the dispersion speeds were smaller. The fluid dynamics of the attractive phase are well understood [8-16], but surprisingly there is no mention in the past studies of the initial violent dispersion of

particles despite the fact that this dispersion is ubiquitous, and occurs for many common liquids and particles.

Though the particle dispersion is ubiquitous it has remained a mystery over many decades. But, this phenomenon has been the root cause of formation of a porous pollen structure known as “pollen rafts” in which an important first step is the initial dispersion of pollen occurring after it comes in contact with the water surface [17]. Cox and Knox [17] did not give a reason for the initial dispersion of pollen.

After this initial dispersion, the pollen particles (usually, form a single anther) cluster to form a pollen raft. It was shown in references [17] and [18] that the formation of porous pollen rafts increases the probability of pollination, because the surface area of the raft is much greater than that of a single pollen grain. Besides, there have been sharp declines in sea grasses of some polluted coastal regions [19,20] that may be associated with surface contamination, which, even when the concentration of contaminants is very small, can influence the porous structure of pollen rafts.

The same way it may be explained why a female of some mosquito species (Culex) has to hold onto the egg raft with its hind legs to prevent it from drifting away while she attaches new eggs. The eggs are laid one at a time and stuck together to form a raft that enables them to float together on the water. If she did not hold onto the raft, it would move away. The eggs of some other mosquitoes (Anopheles) are laid individually onto the water surface; they aggregate under the action of lateral capillary forces with the ends of the eggs touching each other. The spacing between the eggs in this case is relatively larger (which is perhaps advantageous for this species) as they dispersed initially. Lateral capillary forces cause the eggs to cluster and keep them together while the cluster moves around on the water surface. Traveling in large numbers helps ensure survival of the species, because some of the

eggs are eaten by other insects before they hatch.

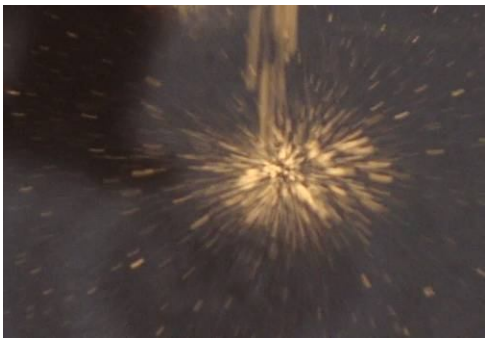

Figure 1.4 Sudden dispersion of flour sprinkled onto water in a dish. Streaklines formed due to the radially-outward motion of the particles emanating from the location where they were sprinkled. The size of flour particles was ~2-100 μm.

This relatively-violent phase, when small particles, e.g., flour, pollen, etc., come in contact (Figure 1.4) with a liquid surface, lasts for a short period of time (only about one second or less on mobile liquids like water) and usually followed by a phase that is dominated by attractive lateral capillary forces during which particles slowly come back to cluster. However, once micron- and nano-sized particles are dispersed, they may remain dispersed since attractive capillary forces for them are insignificant. Small particles may experience other lateral forces, e.g., electrostatic, Brownian, etc., which may cause them to cluster or form, patterns [21-23].

The modeling of interactions among floating particles is a formidable challenge because of the complexity of the interactions and forces involved, i.e., the fluid dynamics of the interface motion, the contact-angle condition on the surface of the particles, the contact-line motion, etc. Recently, a DNS approach was developed for particles trapped at fluid-fluid interfaces [16]. This approach provides not only a capability for resolving the motion of a particle as well as clusters of particles, but also the ability to address the rapidly-changing dynamics of the particles. It is necessary to resolve the particle-level details for particles trapped at fluid-fluid interfaces because the deformation of the interface in between

the particles determines the strength of the lateral capillary forces between them, the latter being one of the main driving forces for their motion. The DNS scheme was used to study two different cases of constrained motions of floating spherical and cylindrical particles. In the first case, the contact angle of floating spheres was fixed by the Young-Dupré law while the contact line was allowed to move to meet the contact-angle requirement. In the second case, the contact line was pinned at the sharp edge of disks (short cylinders) with flat ends; while the contact angle was allowed to change. The angle at the sharp edge was allowed to change within the limits specified by the Gibbs extension to the Young-Dupré law.

The spreading of solid powders on liquid surfaces and of liquids on solid surfaces are common phenomena that we encounter in our day to day life such as laundry, lubrication, wet granulation, dyeing and printing, pharmaceutical and food industries [24-27]. Although thermodynamic predictions for liquids spreading over solid surfaces have been developed for many of these applications [28,29], the mechanism by which solid powders spread over liquid surfaces is not completely understood [30-32].

The spreading behavior of a liquid over a solid surface (or over a liquid with which it is immiscible) is determined by the sign of the spreading coefficient

$$\lambda_{L/S} = \gamma_s - \gamma_l - \gamma_{sl} \tag{1.1}$$

where γ_{sl} is the interfacial tension between the solid and the liquid, and γ_l and γ_s are the interfacial tensions of the liquid and solid, respectively. When the spreading coefficient is greater than zero the liquid spreads spontaneously on the solid surface [29].

It is known that certain powdered materials spontaneously spread on liquid surfaces, just like a liquid on a solid surface. More specifically, the particles of the clump break away, usually a few at a time and move away from the clump to form a monolayer on the liquid surface. In Ref. [29,30] an approach based on interfacial energies that included the work of adhesion due to the polar and non-polar intermolecular interactions was used to obtain an

expression for the spreading coefficient of solid particles on liquids

$$\lambda_{S/L} = 4\left[\frac{\gamma_S^d \gamma_L^d}{\gamma_S^d + \gamma_L^d} + \frac{\gamma_S^p \gamma_L^p}{\gamma_S^p + \gamma_L^p}\right] - 2\gamma_S. \quad (1.2)$$

Here the superscripts d and p refer to non-polar and polar contributions to the surface free energy respectively. Rowe [30] tested the predictions of this model for untreated and surface-treated glass granulated with a number of polymeric binders considered. A positive value of the spreading coefficient implied poor film formation in experiments for the binders considered. Tuske et al. [25] used the spreading coefficients of granules/pellets to select a suitable binding agent for a pharmaceutical application. The friability, an important property of the powder indicating better dispersion, correlated well with the spreading coefficient. He et al. [31] used the same approach to calculate the spreading coefficient of Celecoxib on kollidon 30, HPMC (hydroxypropylmethyl cellulose) and HPC (hydroxypropyl cellulose) that were used as binders. They showed that the positive spreading coefficient of Celecoxib over kollidon leading to formation of open porous granule which facilitates better dispersion of the former, and better dispersion than on HPMC or HPC. They also showed that the spreading coefficient of Celecoxib over HPMC and HPC were negative and hence they did not spread on them.

Nguyen et al. [32] have noted that equation (1.2) for the spreading coefficient of solid particles over liquids is empirical and lacks thermodynamic validity. For example, when the interfacial tension values for PTFE (polytetrafluoroethylene) and water are substituted in equation (1.2), a positive value for $\lambda_{S/L}$ is obtained, suggesting that PTFE would spontaneously spread over water. But, in experiments PTFE does not spread over the surface of a water droplet [28]. They further noted that "The spreading of solid powder over a liquid surface, however, is a very different phenomenon compared to liquid spreading over solid. When a solid powder aggregate expands its apparent coverage over a liquid surface, the

behaviour of the molecules in the powder particles is different from the behaviour of molecules of the liquid as they spread over a solid surface. For a hydrophobic powder, solid powder particles do not increase their surface area as they spread. Instead, powder aggregates merely disintegrate as they move towards the free liquid surface. The only change in this process is that a fraction of the solid powder surface becomes a solid/liquid interface." They emphasized that this important difference has not been addressed sufficiently in the past studies.

Nguyen et al. [32] noted that only when the attractive forces among the particles of a cluster are overcome, its particles can detach to spread over a liquid surface. Since there is no quantitative relation between solid surface free energy and van der Waal forces which exist among the particles holding them together, it is inappropriate to use solid-surface free energy to explain the cohesive work between the particles.

They also calculated the free energy change between the final and initial states when solid particles spread on a liquid surface

$$\Delta G = - A_L \Phi \left(W_{A(LS)} + \beta \left(\gamma_S - \gamma_{LS} \right) \right) \tag{1.3}$$

where Φ is the fraction of the liquid surface that becomes covered by the solid powder, WA is the work of adhesion between liquid and solid. γ_S, γ_L and γ_{SL} are the interfacial energies of the solid, liquid and solid–liquid interfaces, β denotes the ratio of the solid/liquid interface area and the liquid surface area it replaces while touching the liquid surface. They stressed upon the fact that only a fraction of the liquid surface replaced by solid/liquid interface can not be responsible for free energy change of the powder spreading process and hence the original considerations for the "spreading coefficient of solid over liquid ($\lambda_{S/L}$)" does not capture the physical process of powder spreading over a liquid phase. They also have pointed out that the spreading of solid powders on a liquid surface is dominated by the surface

tension of liquid and also emphasized that the phenomena needs to be further investigated.

The rest of the report is organized as follows. In Chapter 2, the experimental methods and in Chapter 3, the direct numerical simulation and the results and in Chapter 4, the force balance of a particle in motion are described which are used to understand and model the process by which particles disperse when they come in contact with a liquid surface. In Chapter 5, the experimental results for the particle dispersion on liquid-liquid interface and the breakup of clump of particles on liquid surface in Chapter 6 are described which is followed by the conclusions.

CHAPTER 2

EXPERIMENTAL METHOD AND RESULTS

There are several factors that determine whether a particle dropped onto the surface of a liquid will sink or float. First, the vertical capillary force must be large enough to balance the particle's buoyant weight. The vertical capillary and pressure forces must also overcome the momentum of the particle, which it possesses before coming in contact with the liquid surface. Since the capillary force acting on a particle varies linearly with the particle size and the buoyant weight and the momentum vary as the third power of the particle radius [33,16], small particles are more easily captured at the interface. Furthermore, to reduce the momentum at impact, particles in the experiments were dropped from a distance of a few millimeters above the interface.

The liquids used in this study are water, corn oil and glycerin. The presence of contaminants on the air-water interface, even when their concentration is very small, can alter the interfacial tension and the contact angle of the water. To address this problem, Millipore water was used. In most of the experiments, particles were spherical; they were dried for several hours at the temperature of 70^{o} C in an oven to eliminate the influence of any residual moisture. Moisture is important because it can influence the contact angle and thus the position of the three phase contact line on the particle's surface. In Figure 2.1b, the top view of two floating glass particles of nearly the same size shortly after they were trapped at the air-water interface is shown. The particle which was dried for several hours was more hydrophobic, and so it floated with more of its surface in the air; even a slight amount of moisture on the surface of a particle can influence the contact angle. After a few minutes, the exposed areas for both particles in became similar. Since the

dispersion phase of the motion of particles sprinkled onto a liquid surface is very short, the surface moisture influences the velocity with which particles disperse. Therefore, for all of the cases for which quantitative data are reported in this paper, particles and powders were dried in an oven to eliminate the influence of the day-to-day variation of the humidity on the dispersion of particles.

In the experiments, one, two or more particles were dropped onto a liquid surface simultaneously. The lateral velocity of particles after they were trapped at the interface was calculated by analyzing the video recordings. Glass particles with diameter between ~10 μm and 1.1 mm, and mustard seeds of ~1.1 mm diameter were used.

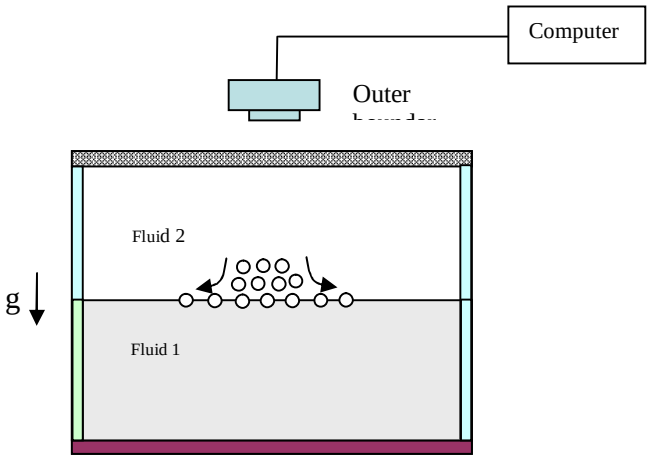

Figure 2.1a Schematic of the experimental setup used to study dispersion of particles which come in contact with a fluid-fluid interface.

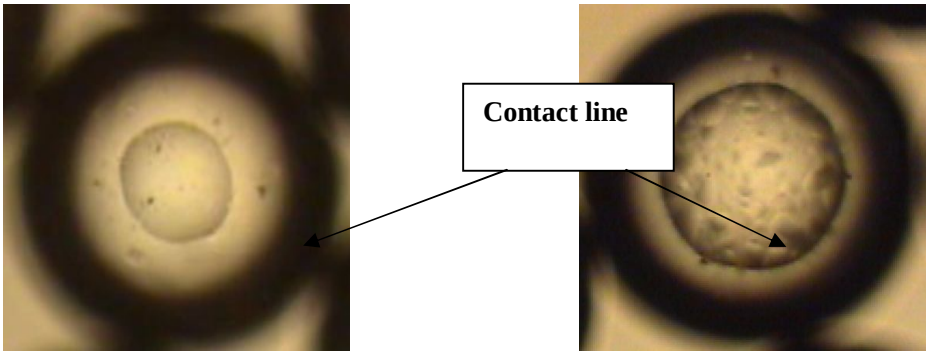

Figure 2.1b Photographs of glass particles floating on the air-water interface (taken from above the surface) showing the influence of humidity on the contact line. The diameter of particles was 550 μm. (left) A particle that was kept under normal room conditions.(right)A particle that was kept in an oven at 70º C for 24 hours. The area exposed to air is larger in the latter and so the dried particle is more hydrophobic.

When a particle comes in contact with a liquid surface, it experiences a vertical force due to capillarity which acts to bring the particle to its equilibrium height within the interface. The equilibrium height can be defined as the distance between the center of mass of the particle and the undisturbed liquid surface (before the particle was sprinkled). The equilibrium height is determined by a balance of the buoyant weight and the vertical interfacial force, and the contact angle which determines the latter force.

The experiments show that when a single spherical particle is dropped onto a liquid surface it causes the fluid around it to move away. The dropped particle is called test particle. The particle itself, of course, does not move laterally on the interface. To investigate the fluid motion caused by a test particle, the interface was seeded with 100 μm sized glass particles. Since the size of these seeded particles was several times smaller than that of the test particle, the assumption is made that they acted approximately as tracer particles and their motion can be used to deduce the local fluid velocity caused by dropping a larger particle. The size of tracer particles compared to that of a test particle, and the field of view/magnification for the camera, were selected so that the motion of

tracer particles within several diameters of the test particle could be monitored. Also, although the number density of tracer particles at the interface was kept small to ensure that they did not influence the fluid motion caused by the test particle, it was large enough to measure the fluid velocity at a sufficient number of points at various distances from the test particles.

2.1 One particle

Figure 2.2 shows the velocity of tracer particles, as a function of the distance from the center of a test glass particle of 850 μm diameter, 0.033 s after contact with the air-water interface. The experiment was repeated for several different spherical particles of the same approximate diameter. After a test particle was trapped at the interface, all of the nearby tracer particles on the air-water interface moved outward from the center of the test particle. The figure shows that the velocity of tracer particles decreased with increasing distance from the test particle. The velocity data points do not fall on a single curve, but are spread about a mean curve. There can be several reasons for this spreading. The surface properties and the smoothness of particles used may be different. The contact line, soon after it was trapped at the interface, was not smooth (Figure 2.1b). There can also be a variation in the particle's rotational velocity, acquired when it was dropped onto the interface.

The velocity of tracer particles decreased with increasing time. For a tracer, initially at a distance of 2.05 mm from the center of the test particle, the velocity at t=0.8 s decayed to approximately zero (Figure 2.3). A particle of radius 1.0 mm attains a velocity of O(10) cm/s normal to the interface under the action of the vertical capillary force. Therefore, the time taken by it to travel a distance equal to its radius downwards is $O(10^{-2})$ s. The test particle, however, oscillates about its equilibrium height for a longer

period before coming to a state of rest. The frequency of oscillation in the experiments for a ~850 μm particle was around 60 Hz. The frequency of oscillation increased with decreasing particle size. Furthermore, the velocity of tracer particles near the dropped particle (~10 mm/s) was an order of magnitude smaller than the estimated value of the velocity of the test particle normal to the interface.

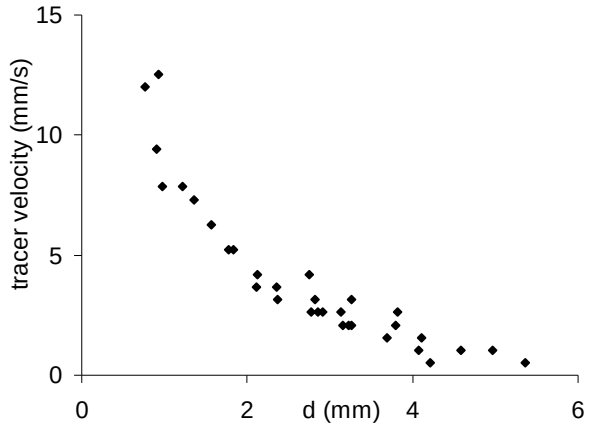

Figure 2.2 The velocity of tracer particles on the air-water interface is plotted as a function of the distance (d) from the center of a test glass particle. The velocity distribution plotted here is at a time 0.033 s after the particle was trapped at the interface. The data were taken for 7 different particles of the same approximate diameter of 850 μm.

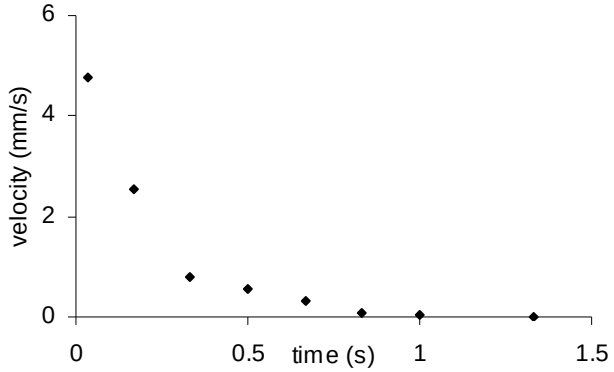

Figure 2.3 The velocity of a tracer particle on the air-water interface initially at a distance of 2.05 mm from a glass test particle of diameter 850 μm is shown as a function of time. The velocity became negligibly small at t = ~0.8 s.

A direct measurement of the latter velocity and an accurate measurement of the frequency of oscillation for particles smaller than ~850 μm was not possible using the present setup.

The above experiment was repeated for a mixture of 60% glycerin in water. The results obtained were qualitatively similar except for that the velocity of tracer particles was smaller. For example, Figure 2.4 shows that the velocity of tracer particles at a distance of 1 mm from the surface of a glass (test) particle of diameter 850 μm for glycerin was ~2 mm/s which is approximately 3 times smaller than on the air-water interface (Figure 2.2). This is expected since the viscosity of 60% aqueous glycerin is about 6 times larger than that of water. The interfacial tension and the density of glycerin are also smaller. The velocity decayed to zero, 0.5 s after the particle was trapped at the interface. This time interval for 60% aqueous glycerin-air interface, as expected, is also shorter than for the air-water interface.

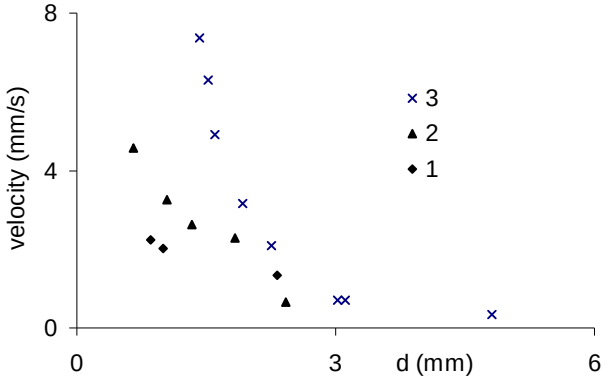

Figure 2.4 The velocity of tracer particles on the surface of a mixture of 60% glycerin in water is shown as a function of the distance (d) from the center of a test particle. The velocity distribution here is at a time 0.033 s after the particle was trapped at the interface. The case marked "1" is for a glass sphere of diameter 850 μm, "2" is for a glass sphere of diameter 550 μm, and "3" is for a mustard seed of diameter 1.1 mm.

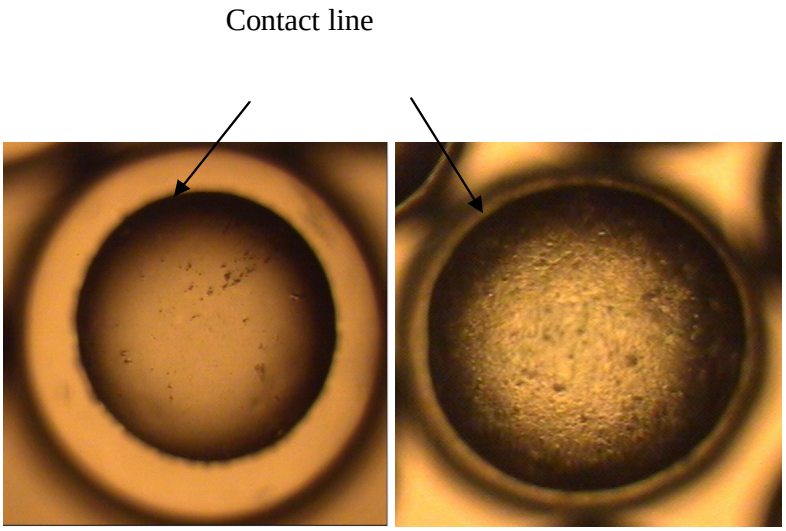

Figure 2.4 (b) The contact line positions for glass particles floating on the surface of 60% glycerin in water are shown. Both particles were dried in an oven for one day. The fraction of the surface of an 850 µm particle exposed to air is smaller than that of 550 µm particle. The dispersion velocity is larger for the latter particles.

The velocity of tracer particles at a distance of 1 mm from the surface of a 550 µm glass test particle was ~3.5 mm/s, as shown in Figure 2.4a. The velocity induced by a 550 µm particle, therefore, was larger than that by an 850 µm glass particle. This could be due to the fact that the fraction of the particle's surface exposed to air was significantly larger for the 550 µm sized particle (Figure 2.4b). The velocity induced due to a mustard seed, at a distance of 1 mm from the particle, was ~4.9 mm/s. This relatively large surface velocity due to a mustard seed is consistent with the fact that it also floated with approximately one half of its surface exposed to air. The frequency of oscillation of a ~1.2 mm mustard seed was about 83 Hz. These results imply that the surface flow induced by the dropping of a particle is greater when it floats so that one half of its surface remains exposed to air. This is also consistent with numerical results and the analysis presented in fore coming chapters.

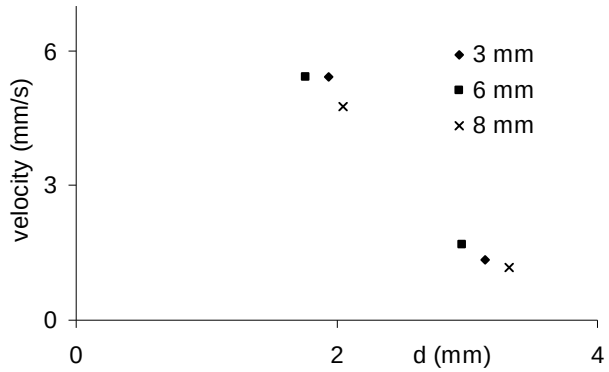

Figure 2.5 The velocity of tracer particles at the distances of ~2.0 and ~3.0 mm from the test particles on the air-water interface. The height from which the test particles were dropped was 3, 6 or 8 mm. The velocity values shown in this figure are at a time 0.033 s after the particle was trapped at the interface. The diameter of the test particles was 850 μm. Notice that the velocity of tracer particles was approximately independent of the height from which the particle was dropped.

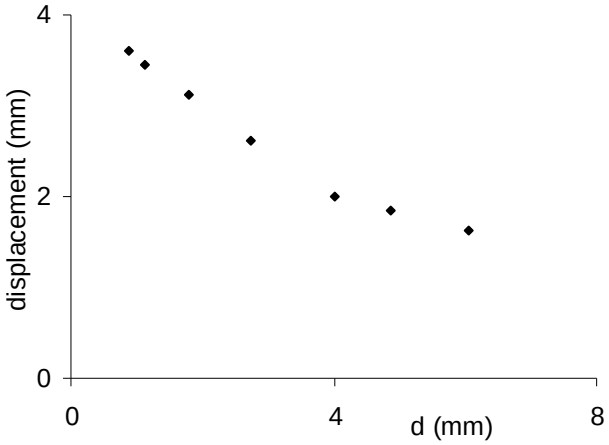

Figure 2.6 The distance traveled by tracer particles on the air-water interface is plotted as a function of their initial distance from the glass test particle. The diameter of the test particle was 850 μm and of a tracer particle was 100 μm.

Next, the results which show that the velocity of tracer particles on the air-water interface due to a test particle was approximately independent of the height from which the particle was dropped when the height was varied between 3 mm to 8 mm are presented. The experimental setup did not allow us to drop the particle from a smaller height. In Figure 2.5, the velocity of tracer particles at the distances of approximately 2 and 3 mm from the test

particle is shown. The Figure shows that the height from which the particles were dropped did not noticeably influence the velocity with which tracer particles moved away from the test particle.

The total distance traveled by a tracer particle (away from the test particle) depended on the initial distance from the test particle. Figure 2.6 shows that a tracer particle initially at a distance of 1 mm from a test particle of diameter 850 μm moved a distance of 3.4 mm and that this value decreased as the distance from the test particle increased. The former implies that a test particle creates a circular space free of tracer particles the radius of which can be more than four times its own diameter. The latter is consistent with the result that the velocity of tracer particles decreased with increasing distance from the test particle.

2.2 Two Particles

The results for the interfacial fluid velocity when two identical glass test particles were dropped simultaneously onto the air-water interface are discussed below. The diameter of the test particles was 850 μm and the initial distance between them was about 910 μm. The motion of tracer particles in this case was radially outward from the middle of the line joining the centers of the test particles; the distance (d) of a tracer particle shown in Figure 2.7 was measured from this point. The velocity of tracer particles as a function of the distance (d) is shown along two mutually orthogonal directions. The inline direction is parallel to the line joining the centers of the test particles and the perpendicular direction is normal to this direction. For a given distance (d), the inline velocity was slightly larger.

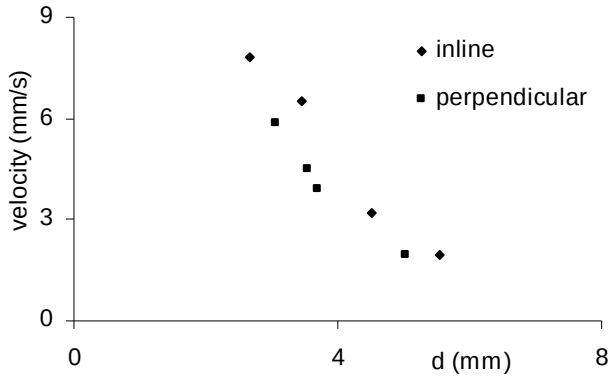

Figure 2.7 The velocity of tracer particles on the air-water interface is plotted as a function of the distance (d) from the mid-point of the line joining the centers of the two test particles. The diameter of the particles was 850 μm and the initial distance between them was 0.91 mm. The velocities shown here are at a time 0.033 s after the particles were trapped at the interface. The velocities of tracer particles are shown along the directions inline (parallel) and perpendicular to the line joining the particles centers.

Furthermore, the velocity of tracer particles in Figure 2.7 was larger than in Figure 2.2 where only one particle was dropped. This implies that the net flow induced at the interface (measured using tracer particles) is stronger when two particles were dropped. This is due to the fact that each particle creates its own radially outward flow, resulting in a net flow which can be approximated as the sum of the flows caused individually by the dropped particles. The other features of the induced flow were qualitatively similar to that for one particle.

After contact with the interface, the two test particles also moved away from each other along the line joining their centers. Figure 2.8 shows that the separation velocity decreased with increasing time, and decayed to approximately zero for t = 0.2 s; the velocities of the two particles were approximately equal in magnitude. The initial distance between the particles was varied to study its influence on the velocity of separation. Figure 2.9 shows that the relative velocity with which particles separated 0.033s after contact, decreased with increasing initial distance between them.

Furthermore, after some time, particles reversed their direction to come back to cluster under the action of attractive lateral capillary forces that arise because of the particles' buoyant weight. The velocity with which they came back however was significantly smaller than the velocity with which they dispersed.

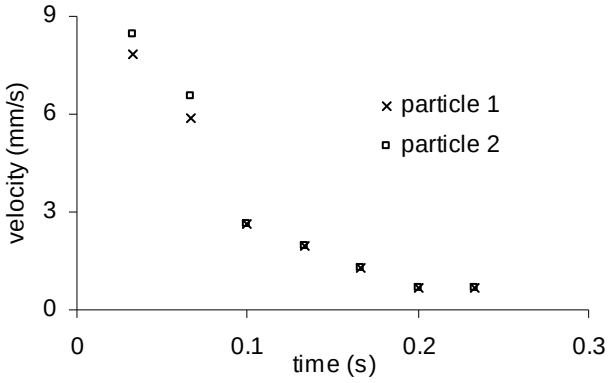

Figure 2.8 The velocity of two glass particles of diameter 850 μm dropped simultaneously onto the air-water interface is shown as a function of time. The initial distance between the particles was 1.21 mm. After becoming trapped in the interface, they moved apart approximately along the line joining their centers. The magnitude of the velocities of the two particles was approximately equal.

The velocity with which two glass particles of the same size moved apart was larger than the velocity with which a tracer particle at the same separation moved away when a single glass particle was dropped. This is noteworthy because the larger glass particles have a larger mass, and so are expected to move slower and not faster. However, they moved apart faster because of a repulsive hydrodynamic force that arises because of their motion in the direction normal to the interface (and so also perpendicular to the line joining their centers). Specifically, when two particles are dropped onto the interface simultaneously, they are pulled downwards into the interface by the vertical components of the capillary forces. If the normal velocities are large, they overshoot equilibrium and oscillate about the equilibrium height before reaching a state of rest. This motion of

particles in the direction perpendicular to the line joining their centers causes the fluid to squeeze through the gap in between them giving rise to the repulsive hydrodynamic force.

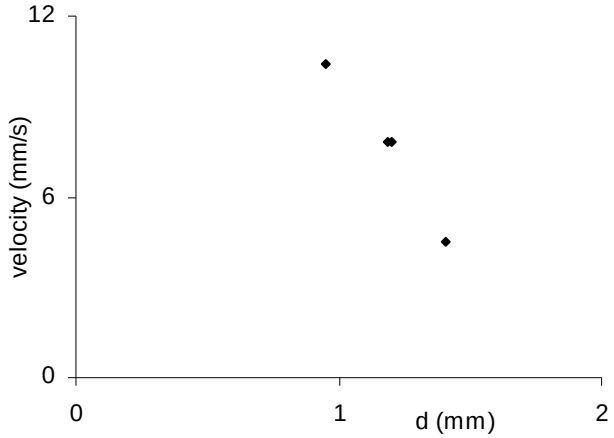

Figure 2.9 The average velocity with which two glass particles dropped together on the air-water interface moved apart along the line joining their centers is plotted against the initial distance between them. The velocities here are at a time 0.033 s after the particles came in contact with the interface. The diameter of particles was 850 μm.

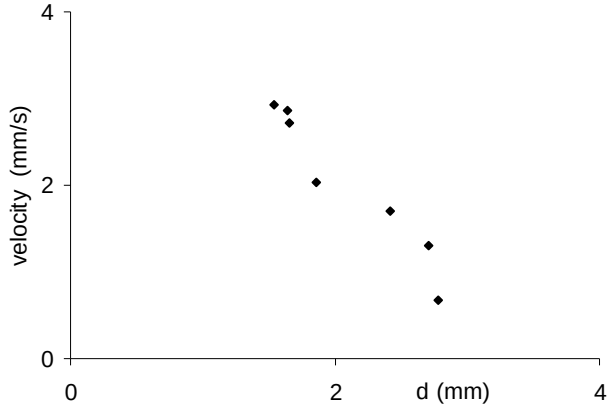

Figure 2.10 The velocity of a glass particle already on the air-water interface induced by dropping of an identical particle is shown as a function of the initial distance between the particles. The diameter of glass particles was 850 μm. The results shown here are at a time 0.033 s after the particle was trapped on the interface.

The case, where a glass particle was dropped near an identical glass particle which was already trapped within the interface was also considered (Figure 2.10). In this case, the trapped particle moved away along the line joining their centers, but the test particle did not move significantly. The particle that is dropped oscillates in the direction normal to the interface and thus creates a flow on the interface away from itself. The particle already at its equilibrium height moved away because of this flow. The velocity with which the trapped particle moved away decreased with increasing distance between the particles. Furthermore, the velocity of the glass particle was smaller than that of a tracer particle at a similar distance. This is not unexpected because the larger glass particles have a larger mass, and hence they move slowly.

2.3 Clusters of Particles

The following discussion is for the case when more than two particles were dropped onto a liquid surface. The goal is to determine the dependence of the dispersion velocity of particles on the number of particles. In Figure 2.11, the velocities of four glass particles dropped together onto an air-water interface as a function of time have been plotted. The diameter of these test particles was 650 μm. The particles moved apart approximately along radial lines emanating from the center of the cluster. The velocities were different because the initial distances between the test particles were not the same and could not be controlled in the experiments. The average velocity with which the particles moved apart was larger for four particles than for two particles. This shows that the velocity with which particles dropped onto a liquid surface move apart depends on the number of particles dropped.

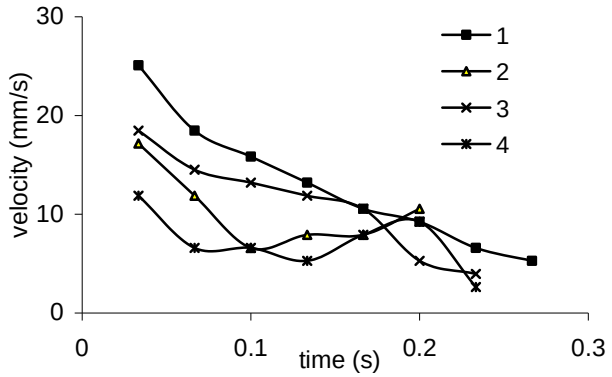

Figure 2.11 The velocities of four glass particles simultaneously dropped onto an air-water interface. The particles moved apart approximately along radial lines emanating from the center of the four particles. The diameter of particles was 650 μm. The initial average distance between the four particles was around 1.0 mm.

To further investigate this increase in the average velocity of dispersion on the number of particles dropped, the cases where a small number of particles, e.g., 2, 4, 8 or 16, were dropped simultaneously were considered. In all of these cases, particles moved away from the center of the cluster after coming into contact with the interface. Video data were analyzed to obtain the average dispersion velocity from their individual velocities. The experiment was repeated several times to obtain an average value of the dispersion velocity.

In Figure 2.12, the average dispersion velocity on the air-water interface is shown as a function of the number of particles dropped. The figure shows that the average velocity increases with increasing number of particles. The same experiment was repeated to study the dispersion of test particles on air-corn oil and air-glycerin interfaces. The results for these latter studies also shown in Figure 2.12 are qualitatively similar. The spreading behavior of glass powder sprinkled onto the air-water interface was also considered. The mean diameter of particles was 18 μm, and the density was 0.6 g/m3. This powder was selected to ensure that a significant fraction of test particles would not

sink. The number of particles dropped for this case was too large to count; hence the amount of powder sprinkled is described in terms of the weight.

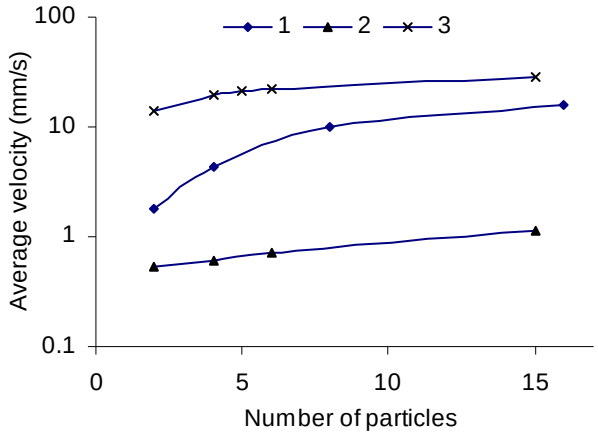

Figure 2.12 The average velocity with which glass particles moved apart 0.033 s after coming in contact with an interface as a function of the number of particles. The case marked "1" is for 850 μm glass particles sprinkled on water, "2" is for 650 μm glass particles sprinkled on 60% glycerin in water, and "3" is for 650 μm glass particles sprinkled on corn oil.

The time taken by a given amount of powder to disperse into a disk shaped region of radius 1 cm is shown in Figure 2.13a. For all of the cases considered, the initial area over which the powder was sprinkled was much smaller than of a circle with radius 1 cm. The time taken decreased when the amount of powder sprinkled increased which implies that the dispersion velocity increases with the amount of powder. For the cluster of the maximum weight considered in this figure, the dispersion velocity was ~ 3 cm/s. This velocity is several times larger than the velocity with which the larger sized glass particles described in Figure 2.2 dispersed. Using the present setup it was not possible to simultaneously drop two particles onto the interface (near each other) if their diameters were smaller than ~400 μm, and so it became unable to study the spreading behavior of two 18 μm sized particles. Particles also dispersed on the corn oil-water interface, but the

speed with which particles dispersed was smaller than on the air-water interface (Figure 2.13b).

The radius of the region covered by the sprinkled powder continued to increase beyond 1 cm, but the rate of dispersion decreased with time before a steady maximum value was reached. In Figure 2.14, the mean radius of the disk shaped region covered by the sprinkled powder against the amount of powder sprinkled is plotted. The radius increased with increasing amount of powder sprinkled until the expansion was inhibited by side walls of the dish.

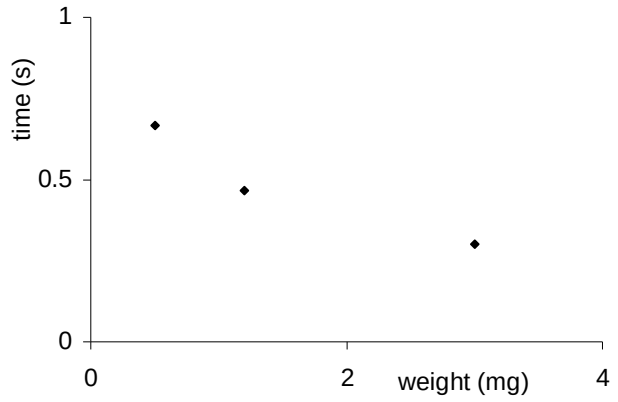

Figure 2.13 The time taken by the powder sprinkled onto the air-water interface to disperse to an approximately circular region of radius 1 cm is plotted against the amount of powder sprinkled. The area of the region over which the powder was sprinkled was relatively small. The average particle size was 18 μm and the density was 0.6 kg/m^3.

It may therefore be concluded that when more particles or a small amount of powder is sprinkled onto a liquid surface, each particle contributes to the outward dispersion of the cluster. The resulting flow on the interface can be approximated as the sum of the flows caused by them individually; therefore the dispersion velocity increases with increasing amount of powder sprinkled.

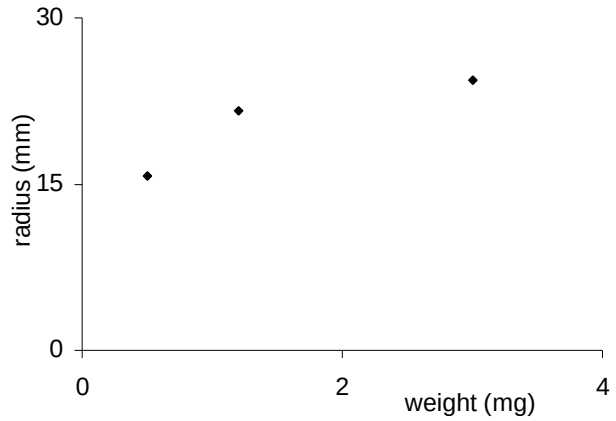

Figure 2.14 The final radius of the disk shaped region covered by the glass powder is plotted against the amount of powder sprinkled. The average particle size was 18 μm and the density was 0.6 kg/m^3.

3.4 Velocity Distribution within a Cluster

To further understand the mechanism by which a group of particles sprinkled onto a liquid surface disperse, clusters of O (100) particles were created and measured their velocities as a function of the distance from the center of the cluster. Initially, the results for mustard seeds of approximately 1.1 mm diameter sprinkled onto the air-water interface are described. In Figure 2.15, the average velocity of particles at various distances from the cluster center is plotted at three different times. At all three times the average velocity increased with increasing distance from the cluster center. In fact, the average velocity at a fixed time increased approximately linearly with increasing distance from the cluster center. Therefore, particles near the outer periphery of the cluster had the maximum velocity and those near the center had the minimum. The average velocity decreased with increasing time as the rate of dispersion decreased. Similar results were obtained when 26 mustard seeds were sprinkled (Figure 2.15b), except that the data were much noisier and the maximum average velocity was smaller. The results for 80 glass beads of diameter 650 μm diameter on 99% glycerin in water are shown in Figure 2.15c. Again, the particle velocity increased with increasing gap

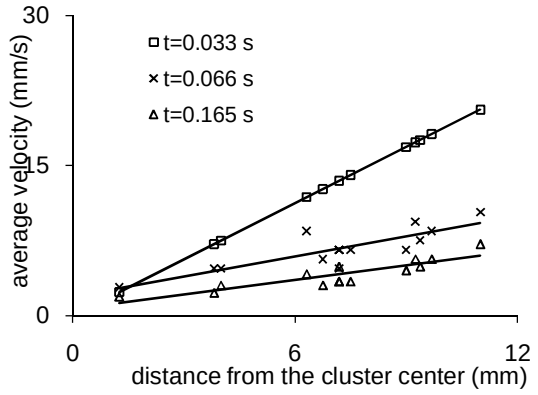

(a)

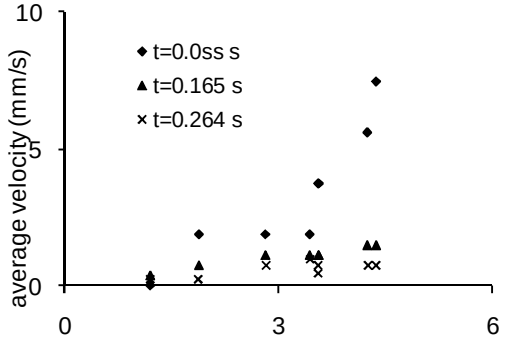

(b)

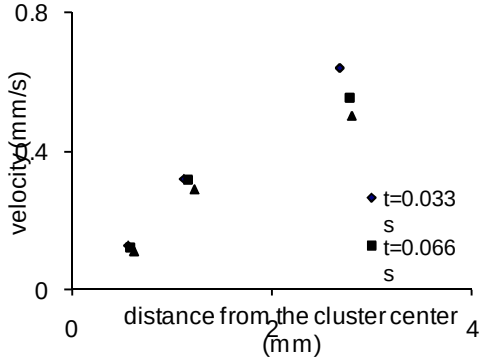

(c)

Figure 2.15 The radial particle velocity is shown as a function of the distance from the cluster center at three different times after they were sprinkled. (a) 76 mustard seeds were sprinkled onto the water surface. (b) 26 mustard seeds were sprinkled onto the water surface. (c) 80 glass spheres of 650 μm diameter were sprinkled onto the surface of 99% glycerin in water.

from the cluster center, and decreased with increasing time. The average velocity for this case was smaller because the glycerin viscosity is larger.

CHAPTER 3

DIRECT NUMERICAL SIMULATIONS (DNS)

In this chapter, the results of direct numerical simulations which were carried out by Singh et al. in [39] for the dispersion of particles trapped at a fluid-fluid interface are detailed. A discussion of these results is included here in order to validate the experimental findings described in Chapter 2. In DNS approach, the details of which were described in [16], particles are moved according to the fundamental equations of motion of fluids and solid particles without the use of models. The fluid-particle motion is resolved by the method of distributed Lagrange multipliers, the interface is moved by the method of level sets and the interface conditions are satisfied using the ghost fluid method [34-37]. The problem of the motion of a contact line on the surface of a particle is modeled using a phenomenological approach in which the contact angle given by the Young-Dupré law is prescribed. In this approach, the contact line on the surface of the particle is moved to maintain the prescribed value of the contact angle. This may not be the case for experiments, especially when the particle velocity is relatively large, if the contact angles for the advancing and receding contact lines are different form the value given by the Young-Dupré law. The initial positions of the particles in the simulations were such that the interface intersected the particles' surface.

To start with, the case of two particles simultaneously released in a fluid-fluid interface is described. The particles centers were at a height of 0.95R above the undeformed interface. The initial shape of the interface was assumed to be flat and the contact line was assumed to be the intersection of the sphere with the flat interface. The

latter was then evolved to satisfy the contact angle condition of 120º. As shown in Figure 3.1, the particles moved downwards under the action of the capillary and gravity forces. The motion of particles caused the fluid around them to move downwards and the interface to deform. The contact angle on the surface of the particles was held fixed at the specified value of 120º. The particles continued to move downwards even after reaching the equilibrium height z=0.4. When their centers moved below the equilibrium height, the direction of the capillary force reversed and it acted upwards against the direction of motion of the particle causing it to decelerate. The maximum velocity attained by the particles before deceleration was 7.9 cm/s. The particles reversed their directions for z= 0.36R.

The particles also moved apart laterally because of the repulsive hydrodynamic forces. These forces arise since the direction of motion of the particles is perpendicular to the line joining their centers and so the fluid is squeezed through the gap between the particles. The lateral velocity (tangential to the undeformed interface) of the particles reached the maximum value after approximately one complete oscillation of the particles about the equilibrium height, and after that the velocity slowly decreased with time. The maximum lateral velocity was around 0.77 cm/s. The maximum velocity normal to the interface was around 7.9 cm/s, an order of magnitude larger than the lateral velocity. After the vertical oscillations of the particles decayed because of the viscous drag and the repulsive hydrodynamic forces that result from these oscillations became smaller than the attractive capillary forces, the particles reversed directions and started to move towards each other. The attractive forces arise because of the deformation of the interface which in the gap between the particles is greater than on the sides. (The deformation of the

interface gives rise to the vertical capillary force that is required to balance the buoyant weight of the particle.) The maximum lateral distance between the particles, before they turned around, was 3.5R, i.e., there was an increase of 0.3R from the initial distance between the particles. The lateral velocity with which two particles came together increased with decreasing distance.

It is well known that the magnitude of attractive lateral capillary force between two particles depends on their buoyant weights [33, 16]. The deformation of the interface due to the particles gives rise to the vertical capillary force which is required for balancing the particles buoyant weights. At the same time, since the deformation of the interface in the region between the two particles is greater, there is a lateral component of the capillary forces on the particles which is attractive and causes the particles to come together. It has been already observed that the experiments show that the tendency of floating particles to disperse after they were sprinkled onto the interface was greater when the area of intersection of the interface and the particle was greater. Moreover, the dispersion velocity was larger for the smaller particles. The smaller particles cause a smaller deformation of the interface and so the attractive capillary forces between them are weaker. This is a consequence of the fact that the capillary forces scale as the radius, whereas the buoyant weight scales as the third power of the radius. Hence, the height or position within the interface of small particles (for which the buoyant weight is negligible) is primarily determined by the contact angle. For example, if the contact angle for a small spherical particle is 90º, it floats so that its center is at the undeformed interface [33, 16].

Therefore, the case where the particle density was one half of that of the lower liquid and the contact angle 85º was considered. Thus, in equilibrium the particles float so that nearly one half of them was above the interface. As before, the particles were pulled downwards by the vertical capillary forces leading to vertical oscillations. As a result of these oscillations, the two particles moved apart. The amplitude of oscillation decreased with increasing time. In this case, since the particles float without causing significant deformation of the interface, the attractive lateral capillary forces between them were much weaker than in Figure 3.1. The particles continued to move apart as shown in Figure 3.3. Simulations were stopped when the distance between the particles was 6.19R.

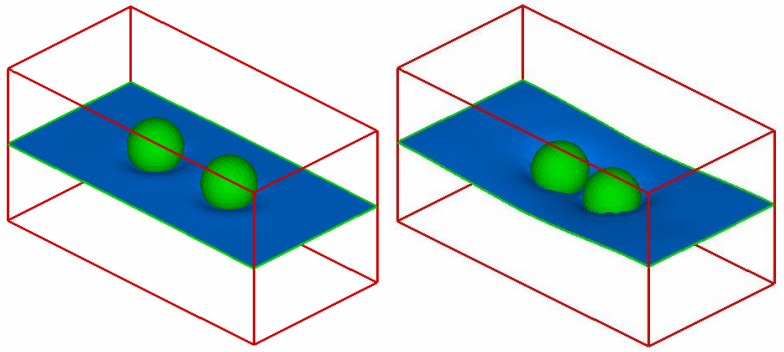

t=0.02 s t=0.26 s

Figure 3.1 Motion of two particles released at the surface. The radius of particles was 0.1 and the contact angle for the particles was 120º. The initial positions of the particle centers were at a height of 0.95R above the undeformed fluid interface. The densities of the particle, and the upper and lower fluids were: 1.1, 0.5 and 1.0 g/cm^3 and the interfacial tension was 4.0 dyn/cm. The interface near the particles deformed to meet the contact angle condition and the vertical capillary force pulled the particles downwards. Initially, the lateral distance between the particles increased. However, as the oscillations normal to the interface decayed and the magnitudes of repulsive hydrodynamic forces decreased, the particles came together under the action of lateral capillary forces.

Next is the case in which one particle was already at its equilibrium height within the interface and the second one was released at a height of 0.95R above the equilibrium height. The latter was pulled downwards by the gravity and capillary forces, while the former

approximately maintained its vertical height (Figure 3.4). The particle that was released above the equilibrium height oscillated about the equilibrium height before coming to rest, but its lateral motion was negligible. However, the particle that was released with its center at equilibrium moved away. This result is similar to that observed in experiments. The maximum lateral velocity of the particle was about one half of the velocity for the case where both of the particles were released at a height of 0.95R above the interface (Figure 3.5).

It has been observed that the lateral velocity with which particles sprinkled onto a liquid surface dispersed increases with increasing number of particles. To study this dependence of the lateral dispersion velocity on the number of particles, the next results are for the case of four particles (Figure 3.6). The particles were released at a height of 0.95R above their equilibrium position within the interface. The initial positions of the particles formed the vertices of a square with sides 3.2R. The initial distance between the neighboring particles was the same as for the two particles case described in Figure S18. The particles were pulled downwards towards their equilibrium height where they oscillated (about the equilibrium height) before coming to rest. The particles also moved apart at the same speed (within numerical errors). Furthermore, the direction of their motion was along diagonals through their centers. The maximum lateral velocity of the particles was about 2.2 times larger than the velocity for two particles (Figure 3.5). This is in agreement with the experimental result that the average velocity with which particles moved apart increases with the number of particles dropped. In experiments, the initial locations of the four particles could not be controlled (i.e., the particles centers did not form the vertices of a square), and so the lateral velocities of the particles with which they moved apart were not the same. However, the average velocity for four particles was

larger than for two. The above DNS results show that when a particle is released above its equilibrium height within the interface the vertical capillary force pulls it downwards causing it to accelerate to a relatively large velocity normal to the interface. Above all,

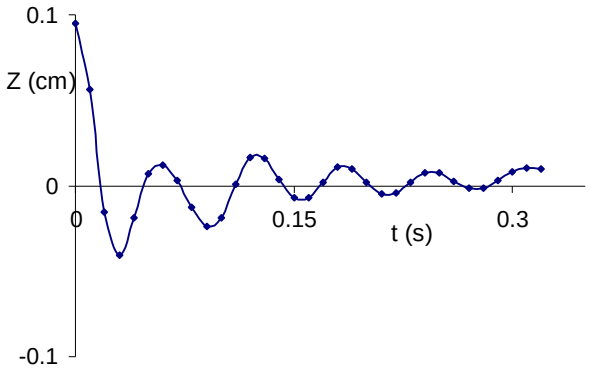

Figure 3.2 The z-coordinate of the particles, obtained from numerical simulation (DNS), is shown as a function of time. The parameters are the same as in Figure 3.3. The particle oscillated about the equilibrium height before coming to rest. The amplitude of oscillations decreased with time. The frequency of oscillation was approximately 16.7 Hz.

since the motion of the particle is inertia dominated, it oscillates several times about its equilibrium height before the viscous drag causes its motion to stop. This motion of nearby particles in the direction normal to the line joining their centers gives rise to the repulsive hydrodynamic forces which cause them to move apart. As the particles velocity in the normal direction to the interface decreases, the magnitudes of the repulsive forces and the dispersion velocity also decrease. Consequently, after some time when the repulsive hydrodynamic forces become smaller than the attractive capillary forces, particles begin to come back together. But, if the buoyant weight of particles is negligible, as is the case for micron and submicron sized particles, then particles only disperse since the attractive capillary forces for them are negligible.

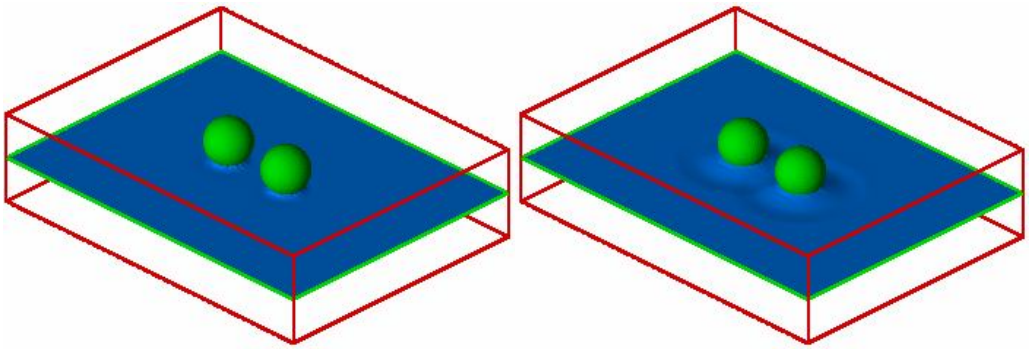

t=0.003 s t=0.005 s

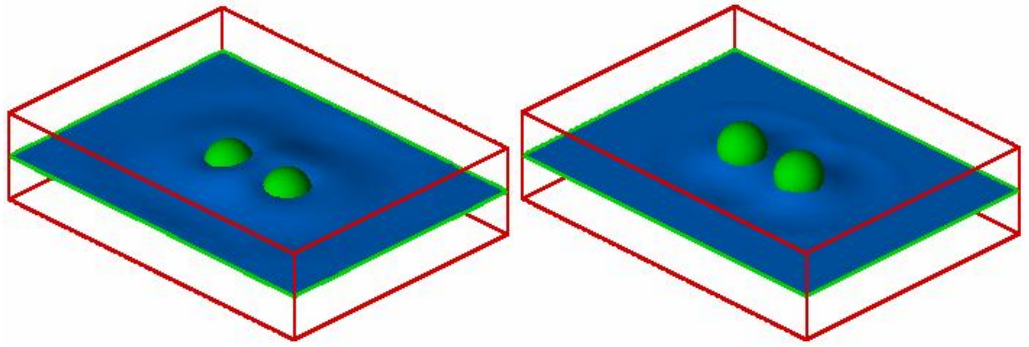

t=0.02 s t=0.06 s

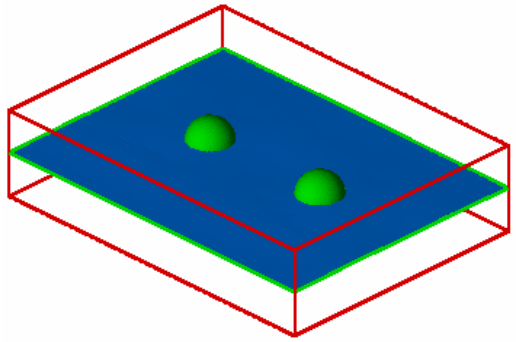

t=0.32 s

Figure 3.3 Direct numerical simulation of the motion of two particles released above their equilibrium height in the interface. The particle radius was 0.1R and the contact angle was 85º. The initial height of the two particles was 0.95R above the undeformed fluid interface. The initial lateral distance between the particles was 3.2R. The densities of the particle, and the upper and lower fluids were: 0.5, 0.1 and 1.0 g/cm^3 and the interfacial tension was 10.0 dyn/cm. The viscosities of the upper and lower fluids were: 0.1 and 1 cP. The interface near the particles deformed to meet the contact angle condition. The resulting vertical capillary force pulled the particles downwards. The particles motion also caused the interface to deform and the waves to develop. The resulting fluid velocity caused the two particles to move apart. For the final figure, the distance between the particles was 6.19R.

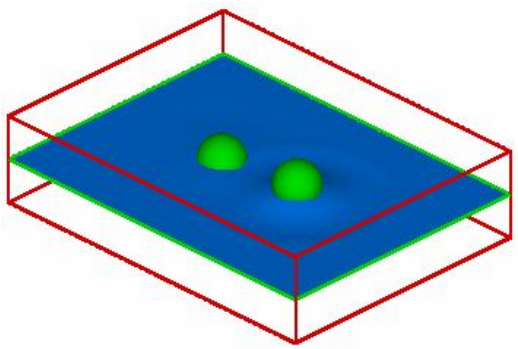

Figure 3.4 The particle on the left was released at its equilibrium height and on the right was released at 0.95R above. The parameters are the same as in Figure 3.3 and t=0.002 s. The vertical oscillatory motion of the latter particle caused the deformation of the interface. The motion also caused the particle released near the equilibrium position to move away.

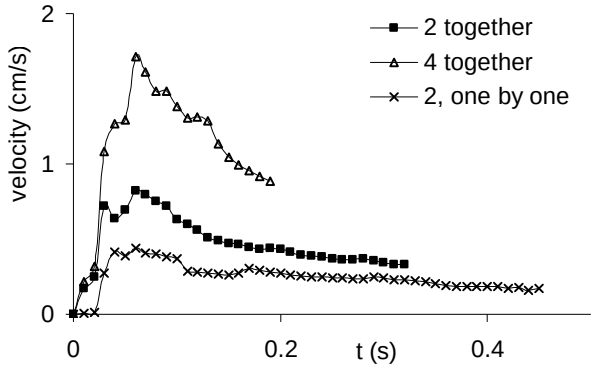

Figure 3.5 The lateral velocity of the particles is shown as a function of time. The parameters are the same as in Figure 3.3. The cases shown are: (i) Two particles released together at a height of 0.95R above the undeformed interface. The initial distance between the particles was 3.2R. (ii) Four particles released together at a height of 0.95R above the undeformed interface. The initial positions of the four particles formed the vertices of a square with sides 3.2R. (iii) One particle released at a height of 0.95R above the undeformed interface, and the center of the second one was at the undeformed interface. The horizontal distance between the particles was 3.2R. The velocity of the latter particle is shown. The velocity of the particle released above the undeformed interface was negligible.

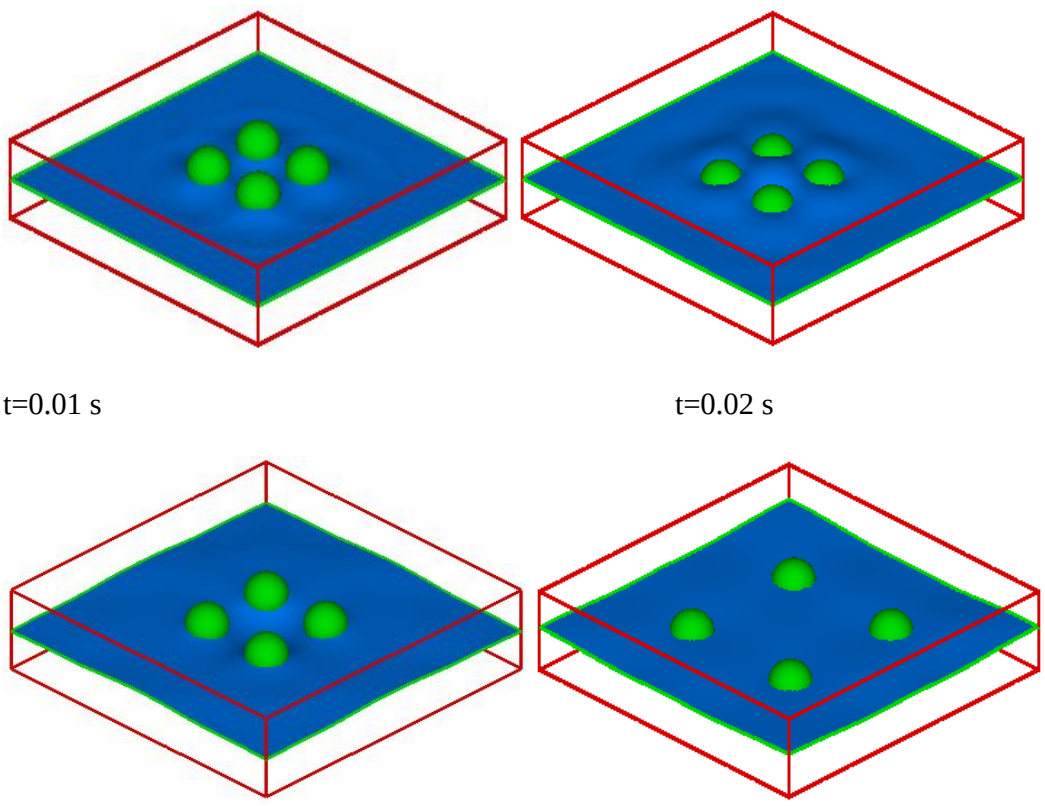

Figure 3.6 Direct numerical simulation of the motion of four particles released above their equilibrium height. The radius of the particles is 1 mm and the initial distance between centers and the undeformed fluid interface was 0.95R; the lower 0.05R of the particles are immersed. The particles were placed on the four vertices of a square with sides 3.2R. The contact angle was maintained at 85º. The other parameters are the same as in Figure 3.3. The interface near the particles deformed to meet the contact angle condition and the vertical capillary force pulled the particles downwards. The particles oscillated about their equilibrium height generating waves on the interface. The particle centers were above the undeformed interface in (i) and (iii), and below in (ii) and (iv). The lateral hydrodynamic forces that arise because of the particles motion normal to the line joining their centers cause the particles to move away from each other. The distance between neighboring particles in the last figure in the sequence was 6.35R.

CHAPTER 4

FORCE BALANCE AND THE EQUATION OF MOTION OF A PARTICLE

This chapter deals with the forces that act on a particle in the direction normal to the interface when it comes in contact with the interface. These forces cause the particle to move towards its equilibrium position within the interface. The main driving forces for this motion are the vertical capillary force and the particle's buoyant weight. The viscous drag resists the particle's motion. The acceleration of the particle under the action of these forces can be written as:

$$m\frac{\mathrm{d}V}{\mathrm{d}t} = \mathrm{F}_{\mathrm{st}} + \mathrm{F}_{\mathrm{D}} + \mathrm{F}_{\mathrm{g}}\,, \tag{4.1}$$

where m is the effective mass of the particle which includes the added mass contribution, V is the particle velocity, F_{st} is the vertical capillary force, F_{D} is the drag, and F_{g} is the gravity force.

The acceleration term in the above equation in terms of the particle's vertical displacement is,

$$\frac{\mathrm{d}V}{\mathrm{d}t} = \frac{\mathrm{d}V}{\mathrm{d}s}\frac{\mathrm{d}s}{\mathrm{d}t} = V\frac{\mathrm{d}V}{\mathrm{d}s} = \frac{\mathrm{d}\left(\frac{V^2}{2}\right)}{\mathrm{d}s}.$$

Here s is measured such that s=0 corresponds to the position in which the particle just touches the interface. Using this in (4.1),

$$m\frac{\mathrm{d}\left(\frac{V^2}{2}\right)}{\mathrm{d}s} = \mathrm{F_{st}} + \mathrm{F_D} + \mathrm{F_g}. \tag{4.2}$$

Integrating the above equation with respect to s, from the particle's initial position (s=0) to the present position s

$$m\left(\frac{V^2}{2} - \frac{V_0^2}{2}\right) = \int_0^s \mathrm{F_{st}}\, ds + \int_0^s \mathrm{F_D}\, ds + \int_0^s \mathrm{F_g} ds \tag{4.3}$$

where V_0 is the initial velocity of the particle. The left side of this equation gives the change in the kinetic energy of the particle, and the terms on the right side respectively represent the work done by the vertical capillary, drag and gravity forces.

The work done by the vertical capillary force can be written in terms of the change in the interfacial energy of the system

$$\Delta A_{12}\, \gamma_{12} + A'_{1p}\, \gamma_{1p} - A_{1p}\, \gamma_{1p} - A_{2p}\, \gamma_{2p}\ . \tag{4.4}$$

Equation (4.4) assumes that the particle is initially immersed in the upper fluid denoted by subscript "1" and the total surface area of the particle is denoted by A'_{1p}, γ_{ip} is the surface tension between the i^{th} fluid and the particle, A_{ip} is the particle's surface area wetted by the i^{th} fluid, ΔA_{12} is the decrease in the surface area between the upper and lower fluids because of the presence of the particle on the interface, and γ_{12} is the interfacial tension between the upper and lower fluids. The energy due to the line tension is assumed to be negligible. It is easy to show that when the deformation of the interface

because of the presence of the particle is negligible [38] for a spherical particle of radius R the above expression reduces to

$$\int_0^s \mathrm{F}_{\mathrm{st}}\, ds = \pi R^2 \gamma_{12} \left(1+\cos\theta\right)^2 \tag{4.5}$$

where θ is the contact angle, as defined by Young's equation: $\cos\theta = \frac{\gamma_{p2} - \gamma_{p1}}{\gamma_{12}}$. The drag force acting on the particle, and thus also the work done by the drag, depends on the particle's velocity. Assuming that the drag is given by the Stokes' law, the work done can be written as:

$$\int_0^s \mathrm{F}_{\mathrm{D}}\, ds = -\int_0^s 6\pi R\mu V\zeta\, ds = -6\pi R\mu \int_0^s V\zeta(s)\, ds. \tag{4.6}$$

Here μ is the viscosity of the lower fluid and $\zeta(s)$ is a factor that accounts for the dependence of the drag on the fraction s of the particle that is immersed in the lower and upper fluids, and the viscosities of the fluids involved. The functional form of $\zeta(s)$ is not known. Also, notice that the velocity V varies as the particle moves normal to the interface. In this work, the Stokes law is used to estimate drag, but other appropriate drag laws can also be used.

The work done by the gravity force is approximately given by

$$\int_0^s \mathrm{F}_{\mathrm{g}}\, ds = \mathrm{Q}\left(\rho_{\mathrm{p}} - \rho_{\mathrm{C}}\right) \mathrm{g}\, s \tag{4.7}$$

where Q is the particle volume, ρ_c is the effective fluid density which changes with s while the particle moves normal to the interface, and ρ_p is the particle density.

After substituting (4.5), (4.6) and (4.7) in (4.3),

$$m\left(\frac{V^2}{2}-\frac{V_0^2}{2}\right) = \pi R^2 \gamma_{12}\left(1+\cos\theta\right)^2 - 6\pi R\mu \int_0^s V\zeta(s)\,ds + \mathrm{Q}\left(\rho_p-\rho_c\right) g\, s \tag{4.8}$$

The above equation for the particle velocity can be simplified further by assuming that the initial kinetic energy of the particle is negligible and using the trapezoidal rule to evaluate the integral term. The former is valid for the experiments because the height from which particles were dropped was only a few millimeters and the particle size was small. Assuming that the drag arises primarily from the portion of the particle immersed in the lower liquid, taking the value to be one half, and $\zeta(s)=1/2$. Then, after simplification,

$$m\frac{V^2}{2} = \pi R^2 \gamma_{12}\left(1+\cos\theta\right)^2 - \frac{6}{4}\pi R\mu Vs + \mathrm{Q}\left(\rho_p-\rho_c\right) g\, s\,. \tag{4.9}$$

The next assumption is that the particle floats so that its center is at the undeformed interface and the effective mass, $m=\frac{4}{3}\pi R^3\rho_p$. For this case, $\theta=\frac{\pi}{2}$ and s = R. The latter assumes that the particle reaches this position for the first time. If the particle oscillates about the vertical position, the distance travelled by the particle will be larger and so will be the work done by the drag force. Using these approximations in the above equation, after simplification,

$$R\rho_p V^2 = \frac{3}{2}\gamma_{12} - \frac{9}{4}\mu V + 2R^2\left(\rho_p - \rho_c\right)g \qquad (4.10)$$

If the interface between the two fluids does not remain flat, then there is an increase in the interfacial area between the two fluids which must be accounted for in expression (4.10). Moreover, if a spherical particle floats (in equilibrium) such that its center is not at the interface, then ΔA_{12} is smaller than πR^2. The interfacial energy available for conversion to the kinetic energy (a fraction of which is acquired by the particle) is smaller for this case. This is consistent with experimental observation that the dispersion velocity was larger for the particles that floated such that the contact line was near their equator.

The solution V of the above quadratic equation is given by:

$$V = \frac{-\frac{9}{4}\mu + \sqrt{\frac{81}{16}\mu^2 + 4R\rho_p\left(\frac{3}{2}\gamma_{12} + 2R^2\left(\rho_p - \rho_c\right)g\right)}}{2R\rho_p} \qquad (4.11)$$

Equation (4.11) gives the particle's velocity after its center reaches the undeformed interface for the first time.

The equation (4.11) implies that the influence of gravity on the velocity decreases with decreasing particle radius. For sufficiently small particles, the velocity increases with decreasing radius and with increasing surface tension, and decreases with increasing viscosity. For example, for $\mu = 0.001$ Pa.s, $\rho_p = 1000.0$ kg/m^3, $\rho_p - \rho_c = 0.1$ kg/m^3 and $\gamma_{12} = 0.07$ N/m, the dependence of the particle velocity on the radius is shown in Figure 4.1. For R=100 μm, V =1.01 m/s, and for R=100 nm, V =23.05 m/s. The figure shows

that when R is smaller than 1 mm the velocity increases with decreasing particle radius. The latter is an expected result because the capillary force acting on a particle varies linearly with the radius whereas the particle's mass varies as the third power of the radius. Therefore, the velocity attained by a particle due to the capillary force increases with decreasing particle radius. In the limit R approaching zero, the velocity is given by

$$V = \frac{2\gamma_{12}}{3\mu} \tag{4.12}$$

This is the maximum velocity that can be attained by a particle under the action of the vertical capillary force. For the air-water interface, the maximum velocity attainable (under the assumptions stated above) is 46.67 m/s.

The above velocity can be used to estimate the time taken to move a particle initially touching the interface to a position where its center is at the undeformed interface; for R=100 μm, the time taken is of $O(10^{-4})$ s, and for R=1 μm, it is of $O(10^{-7})$ s.

It is noteworthy that the work done by the drag force is significant only when the particle moves over a much longer distance, the fluid viscosity is relatively large, or the velocity is sufficiently large; otherwise the decrease in the interfacial energy due to the capture of the particle at the interface is mostly converted into the kinetic energy. The velocity for this can be obtained from (4.10) by neglecting the drag and gravity terms, which gives

$$V = \sqrt{\frac{3\gamma_{12}}{2R\rho_p}}. \tag{4.13}$$

Equation implies that the particle velocity increases with decreasing particle radius, and in fact diverges as the radius approaches zero. However, since the work done by the drag force increases with increasing particle velocity, the velocity for small

particles does not diverge, but is given by the balance of the viscous drag and the vertical capillary force. Furthermore, if the fluid viscosity is sufficiently large, the particle velocity remains small and the particle does not oscillate before coming to a state of rest. Thus, particles sprinkled onto the surface of a very viscous liquid are less likely to disperse.

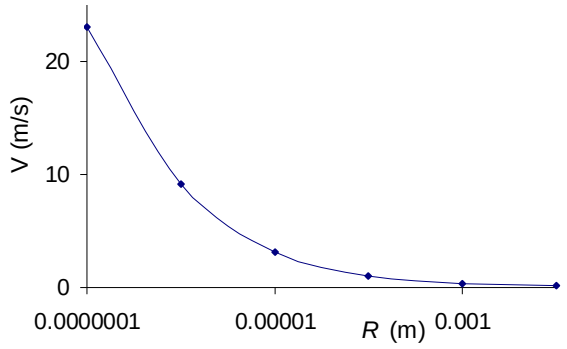

Figure 4.1 The velocity of a spherical particle normal to the interface given by equation (4.11) is plotted as a function of the particle radius. The parameter values were assumed to be: $\mu = 0.001$ Pa.s, $\rho_p = 1000.0$ kg/m^3, $\rho_p - \rho_c = 0.1$ kg/m^3 and $\gamma_{12} = 0.07$ N/m.

It is reminded that the above analysis assumes that the equilibrium position of the particle center is at the undeformed interface and that the interface around the particle is flat. If, however, the interface around the particle is not flat, the decrease in the area between the upper and lower fluids due to the presence of the particle will be smaller than the area of intersection between the particle and the flat interface and the discrepancy must be included in equation (4.11). An increase in the interfacial area between the fluids due to the deformation of the interface implies that the interfacial energy available to drive the motion of the particle is smaller, and thus the maximum velocity attained by the particle will be smaller. Furthermore, even if interface around the particles is flat at equilibrium, this may not be the case when it reaches this position for the first time

because the particle and the fluid velocities are not zero and as a result the interface contains waves. The interface can become flat only after both the particle and the fluid stop moving.

Direct numerical simulations show that the particle oscillates about the equilibrium several times before coming to rest (Figure 4.2). This is due to the fact that the motion of particle is inertia dominated. Thus, when the particle reaches the equilibrium height, its velocity is non-zero, and so it continues to move downwards. However, when the particle center moves below the equilibrium height, the vertical capillary force changes direction and acts upwards to bring the particle back to the equilibrium. The viscous drag acts throughout this process to slow the particle.

To study the above behavior of the particle motion, equation (4.1) for the motion of the particle considered. The approximations stated above are used to simplify (4.1), i.e., those used for obtaining (4.10). The surface tension force will be obtained by assuming that the particle is spherical and that the contact angle is equal to its equilibrium values. The drag force will be assumed to be given by the Stokes formula, as discussed above, and the buoyancy force only depends on the particle's vertical position. Under these assumptions, equation (4.1) can be written as

$$m\frac{\mathrm{d}V}{\mathrm{d}t} = -2\pi\left(R\sin\theta_c\right)\gamma_{12}\sin\left(\theta_c+\alpha\right) - 6\pi\mathrm{R}\mu V\zeta(s) + \mathrm{Q}\left(\rho_{\mathrm{p}}\text{-}\rho_{\mathrm{c}}\right)\mathrm{g} \qquad (4.14)$$

Here θ_c is the angle between the vertical and the contact line on the sphere's surface and

α is the contact angle.

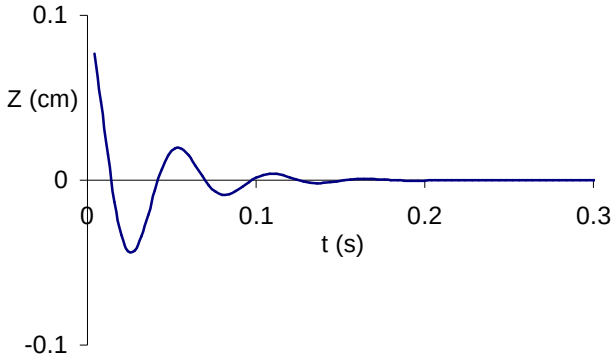

Figure 4.2 The z-coordinate of the particle center obtained numerically by solving (4.14) is shown as a function of time. The radius of particle is 0.1 cm. Initially, the particle center is at z=0.95R (above the interface). The remaining parameters are the same as in Figure 3.3. The particle oscillates about the equilibrium position (z=0) before coming to rest. The amplitude of oscillations decreases with increasing time. The frequency of oscillation is approximately 17.9 Hz.

A time dependent numerical solution of the above differential equation is shown in Figure 4.2. The parameter values used were the same as for the numerical results presented in Figure 3.2. The figure shows that the particle oscillates about the equilibrium height several times while the amplitude of the oscillations decays with time because of the viscous drag. These results are qualitatively similar to those in Figure 3.2 obtained using the DNS approach. But, there are also some differences. The frequency of oscillation given by the two approaches differed by about 7% and the rate of decay of oscillations was slower for the DNS results. This perhaps is due to the fact that the interface is allowed to deform in the DNS approach, but is assumed to be flat in the derivation leading to equation (4.14). The interface deforms because of the vertical oscillations of the particles.

Equation (4.14) is a linear ODE with variable coefficients. To show that it is equivalent to the equation for a spring-dashpot system, equation (4.14) is linearized about the equilibrium position, z=0. To do this, the contact angle is assumed to be $\alpha = \frac{\pi}{2}$, $\theta_c = \frac{\pi}{2}$ and $\zeta(s) = 1/2$. After linearization, it becomes

$$\frac{4}{3}R^3\rho_p\frac{\mathrm{d}^2Z}{\mathrm{d}t^2} + 3\mathrm{R}\mu\frac{\mathrm{dZ}}{\mathrm{d}t} + 2\gamma_{12}Z + R^2\left(\rho_\mathrm{p}-\rho_\mathrm{c}\right)\mathrm{g}\,\mathrm{Z} = 0. \tag{4.15}$$

where Z is the particle's position. The above second order linear ODE is equivalent to a spring-dashpot system. Its solution can be written as:

$$Z = Z_0 e^{kt} \tag{4.16}$$

where

$$k = \frac{-3R\mu \pm \sqrt{D}}{\frac{8}{3}R^3\rho_p}$$

$$D = 9R^2\mu^2 - \frac{16}{3}R^3\rho_p\left(2\gamma_{12} + R^2\left(\rho_\mathrm{p}-\rho_\mathrm{c}\right)g\right)$$

The nature of the solution depends on the sign of discriminant D. If the sign is positive, then k is real and negative for both of the roots. In this case, the solution decays exponentially with time to zero. This is expected to be the case when the fluid viscosity is sufficiently large. If the sign of D is negative, then k is complex and so the solution is oscillatory. The frequency of oscillation is given by

$$\omega = \frac{3\sqrt{-9R^2\mu^2 + \frac{16}{3}R^3\rho_p\left(2\gamma_{12} + R^2\left(\rho_\mathrm{p}-\rho_\mathrm{c}\right)g\right)}}{16\pi R^3\rho_p}. \tag{4.17}$$

The real parts of both of the roots are negative and so both of the solutions decay exponentially to zero. The time constant τ of the solution, i.e., the time taken by the solution to decay by a factor of e^{-1}, is given by

$$\tau = \frac{8R^2\rho_p}{9\mu} \tag{4.18}$$

The time constant decreases with decreasing particle size and with increasing viscosity. Therefore, the vertical oscillations of a trapped particle decay faster when the radius is smaller and the viscosity is larger. Using the parameter values in Figure 4.1, for a particle of radius 1 mm, the time constant is 0.9 s, and for a 10 μm sized particle it is $9.0\text{x}10^{-5}$ s. It is worth to remember that the former estimate of the time constant is smaller than for direct numerical simulations for which the interface is allowed to deform. Also notice that as R becomes small there is a critical value of R for which D becomes positive. For these parameter values, the critical value of R is ~12 nm. The imaginary part of the root gives the frequency of oscillation. For the parameter values listed in Figure 4.1, the frequency of oscillation (ω) in Hz is plotted as a function of the particle radius in Figure 4.3. The frequency increases with decreasing particle radius. For R=1 mm, ω = 51.6 Hz; for R=10 μm, $\omega = 5.2\text{x}10^4$ Hz; and for R=100 nm, $\omega = 5.1\text{x}10^7$ Hz.

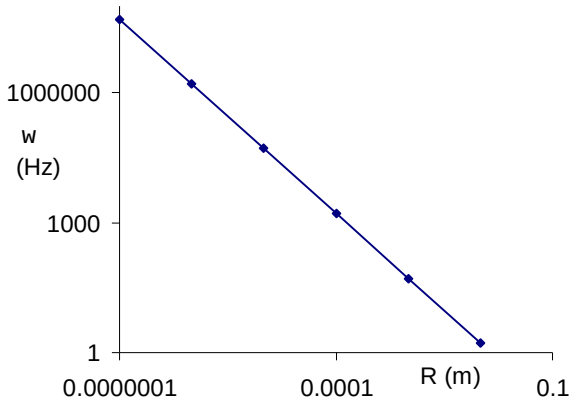

Figure 4.3 The frequency (ω) of oscillation of the solution given by equation (4.16) is plotted as a function of the particle radius. The parameter values are the same as in Figure 4.1.

CHAPTER 5

PARTICLE DISPERSION ON FLUID-LIQUID INTERFACES

In this chapter, the dispersion of particles on the fluid-liquid interface is described. In the previous chapter it was shown that when small particles, e.g., flour, pollen, etc., come in contact with an air-liquid interface, they disperse in a manner that appears explosive. In the case of the dispersion on a liquid-liquid interface, it is relatively weaker than on an air-liquid interface, and occurred over a longer period of time. This is a consequence of the fact that particles became separate while sedimenting through the upper liquid and reach the interface over a time interval that lasts for several seconds. The rate of dispersion depended on the size of particles, the particle and liquids densities, the viscosities of the liquids involved, and the contact angle. For small particles, partial pinning and hysteresis of the three-phase contact line on the surface of the particle during adsorption on liquid-liquid interfaces is also important. The frequency of oscillation of particles about their floating equilibrium increased with decreasing particle size on both air-water and liquid-liquid interfaces, and the time taken to reach equilibrium decreased with decreasing particle size. These results are in agreement with our analysis.

5.1 Dispersion and Clustering of Two Plastic Beads on Air-water Interface

As discussed in the initial chapter, when small particles come in contact with a liquid surface they immediately disperse. This relatively-violent phase, which lasts for a short period of time (only about one second or less on mobile liquids like water), is usually followed by a phase that is dominated by attractive lateral capillary forces during which

particles slowly come back to cluster where as once micron- and nano-sized particles are dispersed, they may remain dispersed since attractive capillary forces for them are insignificant. Small particles may experience other lateral forces, e.g., electrostatic, Brownian, etc., which may cause them to cluster or form patterns.

To illustrate the phenomena described above, let us consider the case of two plastic beads as shown in Figure 5.1(a), which were simultaneously dropped onto the water surface. The beads first moved apart and then came back together. The former phase, which is the primary focus of this chapter, is discussed below. The latter phase is due to attractive capillary forces that arise because of the deformation of the interface by the trapped beads, as they are heavier than water. More specifically, the floating beads experience attractive capillary forces because the interface height between them is lowered due to the interfacial tension. Notice that the speed with which the beads dispersed was about six times larger than the maximum speed attained during the clustering phase. The time duration for which the beads moved apart was about one third of the time they took to cluster. As noted in the figure caption, to ensure that these results were not influenced by contamination, e.g., surfactant, the experiment was repeated many times using the same beads while the water used in the test was changed.

5.2 Experimental Setup

The liquids used in this study were Millipore water, corn oil and decane. Millipore water was used to ensure that contaminants were not present as even when their concentration on the air-water interface is very small they might change the interfacial tension and the contact angle of the liquid. Furthermore, glass particles were thoroughly rinsed in water and then dried for several hours at the temperature of 70º C in an oven to

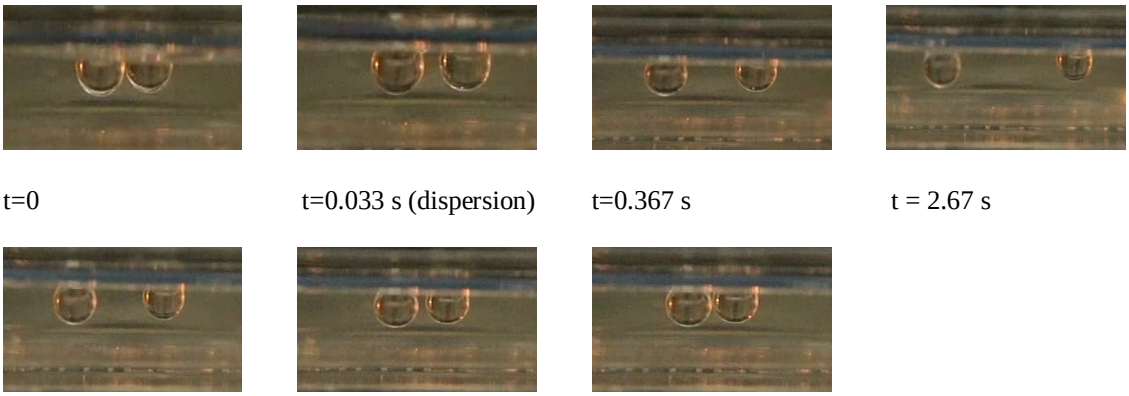

Figure 5.1(a) Dispersion and clustering of two plastic beads on the air-water interface. The diameter of beads was 4.46 mm. The beads were carefully washed in water many times. The experiment was repeated more than 30 times with fresh Millipore water, and the Petri dish used in the experiment was rinsed with Millipore water every time, to ensure that contamination was not a factor and that this behavior of the beads did not change with time.

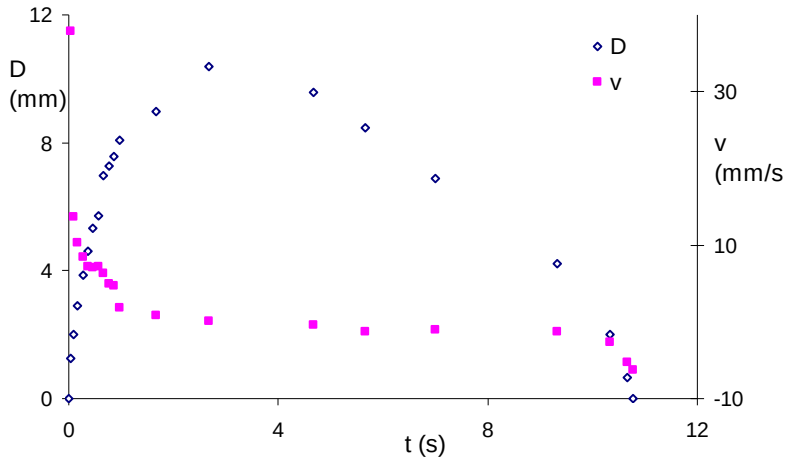

Figure 5.1(b) The gap (D) between the beads and the velocity (v) with which they are moving apart after they came in contact with the interface are shown as a function time. The gap initially increased as the beads moved apart and then decreased as they clustered under the action of lateral capillary forces. The maximum velocity with which the beads moved apart was about six times larger than the maximum velocity with which they came together.

overcome the influence of any residual moisture which could influence the contact angle and hence the position of the three-phase contact line on the particle's surface. It may be noted that water and decane, and water and corn oil, are immiscible, and that the three liquids have different densities which resulted in the formation of horizontal liquid layers. For example, since decane is less dense than water, the decane was in the upper layer and the water in the lower layer. The density of water, corn oil and decane are 1000 kg/m3, 922 kg/m3 and 726 kg/m3, respectively. The viscosity of water, corn oil and decane are 1.0 cP, 65.0 cP and 0.92 cP, respectively. The interfacial tension between air- water was 72.4 mN/m, decane-water was 51.2 mN/m, and corn oil-water was 33.2 mN/m.

The horizontal positions of particles were recorded using a digital video camera connected to a Nikon Metallurgical MEC600 microscope and the vertical positions of particles using a high-speed camera (Casio Exilim F1) mounted on the side, as shown in figure 5.2. The latter positions evolved much more rapidly and therefore a high speed camera was needed to resolve the motion. For example, the frequency of oscillation during adsorption for the particles investigated in this study was approximately between 20-120 Hz.

The distance between the particles was measured by analyzing the movies frame-by-frame with a calibrated digital ruler. The particles were released very close to the surface of the upper liquid (about 1 mm above the surface). This was done to ensure that their speed before touching the interface was small. The vertical and horizontal positions of particles were measured as a function of time by analyzing the video recordings. The fluid velocity at the interface was measured by tracking small tracer particles trapped on the interface.

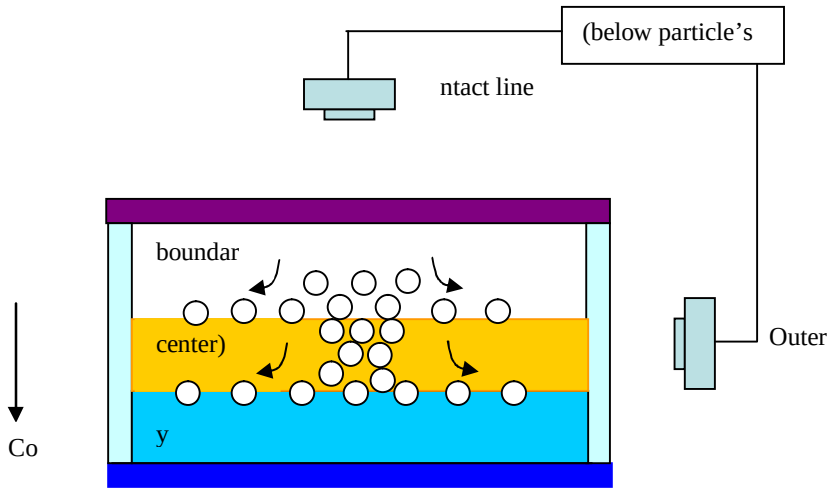

Figure 5.2 Schematic of the experimental setup used to study the dispersion of particles on a fluid-liquid interface.

5.3. Transient Motion of Particles During Their Adsorption

As discussed earlier, the analysis and direct numerical simulations show that while particles are being trapped on the surface of a mobile liquid they oscillate about their equilibrium positions before reaching a state of rest and that this results in a radially-outward flow on the interface away from the particle which causes tracer and other particles on the interface to move away. To investigate these oscillations and the resulting interfacial flow, the video recordings of the motion of particles after they came in contact with the interface were analyzed. The particle size was varied between approximately 5 μm and 4 mm. The behavior was investigated for the air-water, oil-water and decane-water interfaces. The first case which is described is when a single particle comes in contact with a fluid-liquid interface which is followed by a discussion of the cases when two particles and a cluster of particles come in contact with the interface.

5.3.1 Adsorption of a Single Particle

The motion of a 2 mm spherical plastic bead from the time it came in contact with the decane-water interface is shown in figure 5.3. The bead released in the upper liquid slowly sedimented to the decane-water interface, and once it came in contact with the interface it was pulled downwards by the vertical capillary force. The bead continued to move downward even after reaching the equilibrium height. However, when this happened the vertical capillary force reversed its direction, and thus after travelling some additional distance the direction of bead's motion also reversed. The bead oscillated three times about its equilibrium position before its motion became indiscernible. Since the bead overshoots and oscillates about the equilibrium position before stopping, it may be concluded that its motion is inertia-dominated and similar to that of an underdamped mass-spring-dashpot system. The motion of the bead also caused ring-shaped interfacial waves that moved away from the bead and slowly dissipated.

A similar behavior was observed for a plastic bead released above the air-water interface (Figure 5.4) and a mustard seed released above the decane-water interface (Figure 5.5). Notice that since the mustard seed was hydrophobic its floating height was relatively greater than that of the plastic bead. The behavior of a lighter plastic bead (less dense than the loitr liquid) shown in Figure 5.6, which rose to the air-water interface, was also similar. Notice that the frequency of oscillation for these cases was 20 Hz or larger, and therefore a high speed camera was needed to see and analyze them.

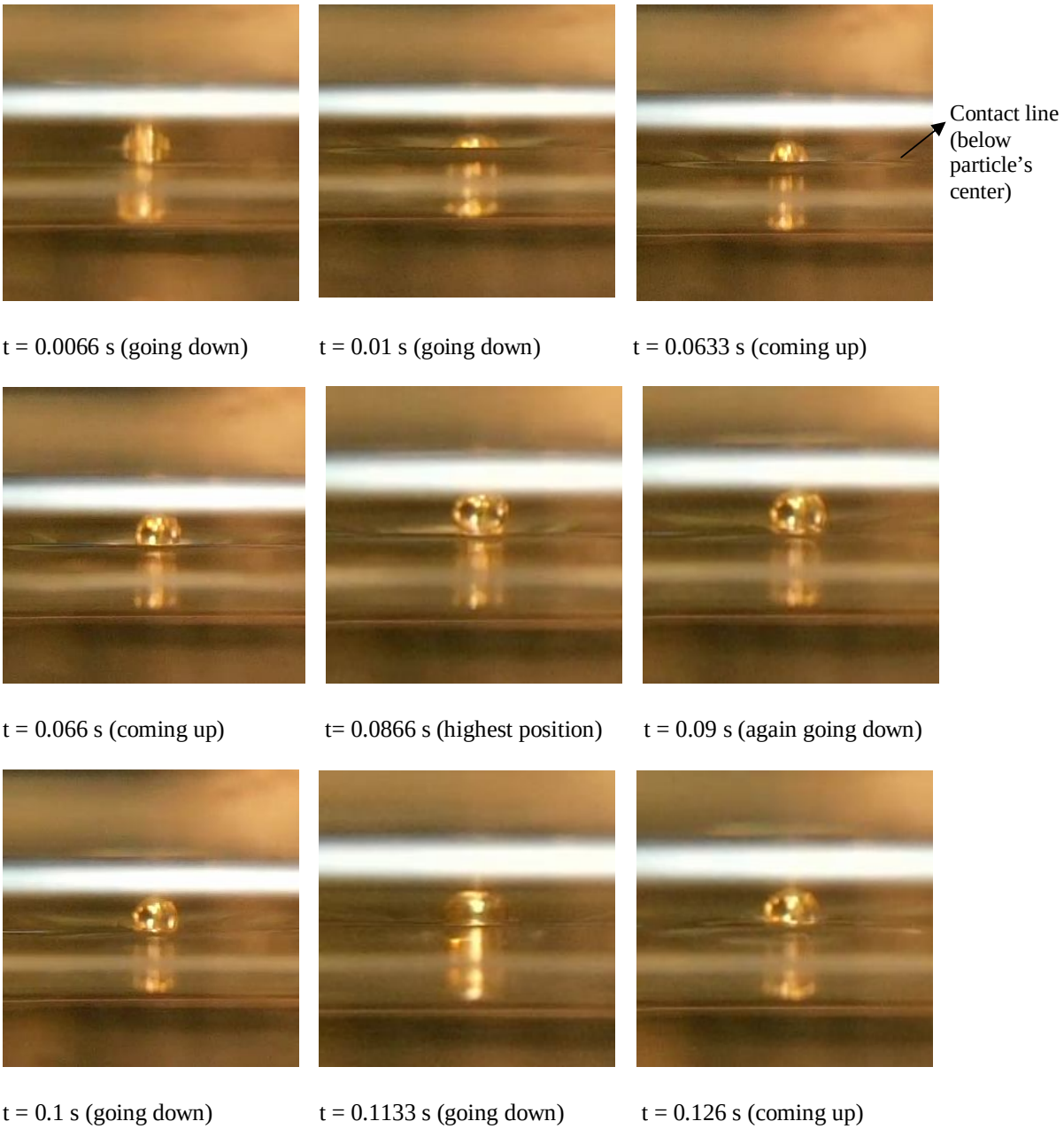

Figure 5.3 Trapping of a spherical plastic bead of 2 mm diameter on the decane-water interface. The bead oscillated about its equilibrium position before its motion stopped. The sequence shows the phenomenon from the time the bead touched the interface to the time it reached the equilibrium position.

t=0 s (going down)

t=0.0066 s (going down)

t=0.01 s (going down)

t=0.037 s (lowest height)

t=0.047 s (going up)

t=0.06 s (going down)

t=0.073 s (going up)

Figure 5.4 Trapping of a plastic bead of 2 mm diameter on the air-water interface. The bead oscillated about equilibrium before its motion stopped. Notice that the equilibrium floating height of the bead is lower than in Figure 8 for the decane-water interface.

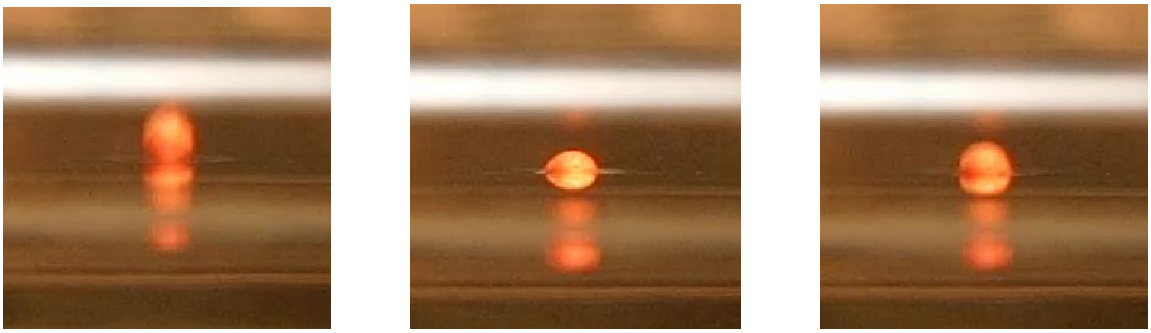

t= 0.0066 s (going down) t = 0.0133 s (going down) t= 0.0466 s (going up)

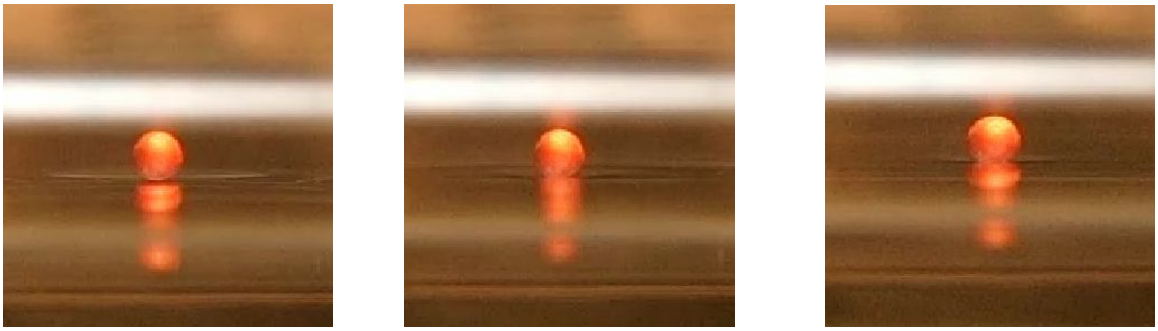

t=0.0566 s (top position) t = 0.0233 s (again going down) t=0.066 s (going up)

Figure 5.5 Trapping of a mustard seed of 1.36 mm diameter on the decane-water interface. The mustard seed oscillated about equilibrium before its motion ceased.

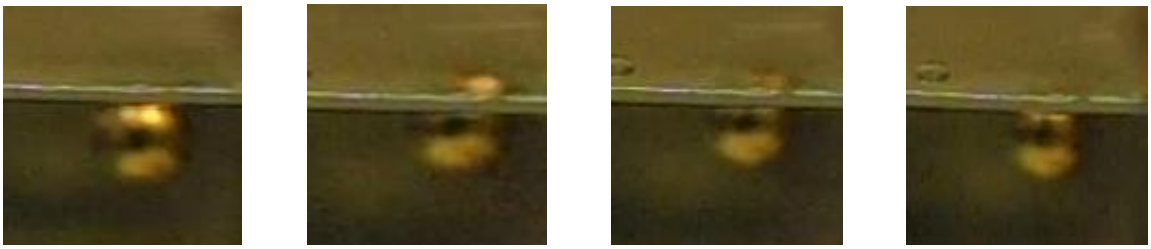

t=0 (going up) t= 0.0166 s (going up) t=0.02 s (going down) t=0.027 s

t=0.04 s (going up) t=0.0633 s (going down)

Figure 5.6 Trapping of a plastic bead of 2 mm diameter on the air-water interface. The bead was released below the water surface. It rose to the air-water interface and oscillated about the equilibrium position before its motion ceased.

The photographs shown in Figures 5.3 to 5.6 were taken from high-speed movies of particles undergoing adsorption at the fluid-liquid interfaces. These movies were also analyzed frame-by-frame to obtain the dimensionless distance of the center of particles (Z/R) from the undeformed interface as a function of time. The latter results for a 650 μm glass bead are shown in Figure 5.7 for the air-water and decane-water interfaces. Figure 5.7a shows that the equilibrium height of the center of the particle relative to the undeformed interface is lower on the air-water interface. This can be also seen in Figure 5.7b which shows that the particle floats on the decane-water interface such that a smaller fraction of it is immersed in the water, whereas on the air-water interface a larger fraction of its lower surface is immersed in the water. This is expected since for the same floating height the buoyant weight of the particle on the air-water interface is larger, and thus to

balance its weight it is more immersed in the lower liquid. The angle of the three-phase contact line on the particle's surface is another important parameter, but its value is not known to us.

It is noteworthy that even after the vertical oscillations of the particle subsided, its floating height on the decane-water interface slowly decreased before reaching a constant value. This is due to the partial pinning of the contact line on the particle's surface and the contact angle hysteresis (Figure 5.7a). This issue is discussed below in more detail. Also notice that the amplitude of oscillation of the particle was larger on the decane-water interface. This is because the densities of decane and water are closer than the densities of air and water, hence the restoring buoyant force resulting from a displacement away from the equilibrium position is smaller for decane and water.

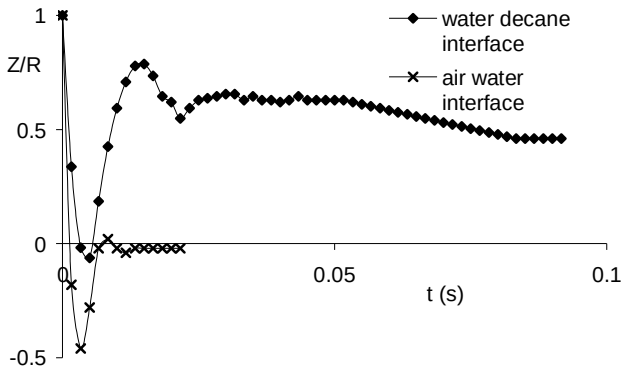

Figure 5.7(a) Trapping of a 650 μm glass particle on the air-water and decane-water interfaces. The dimensionless vertical positions (Z/R) as a function of time. Here Z is measured from the undeformed interface.

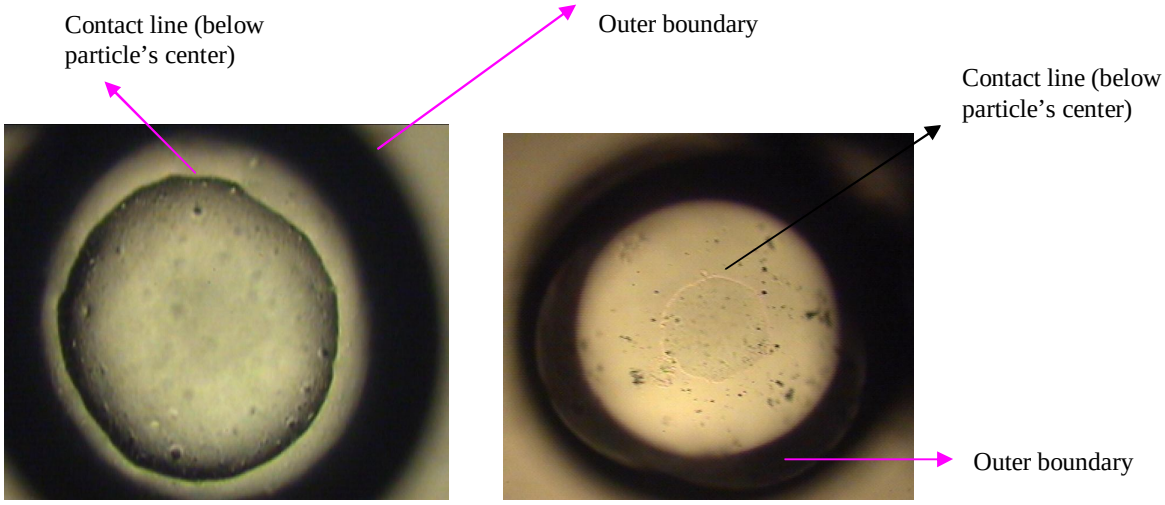

(b)

Figure 5.7(b) The contact lines on the air-water and decane-water interfaces for the particle.

When the diameter of glass particles in the experiments was approximately 650 µm or larger, a significant fraction of the sprinkled particles were not captured on the corn oil-water interface and those that were captured did not disperse. This was also the case for millimeter-sized mustard seeds and plastic beads. Smaller glass particles were captured, and as discussed below, after they were captured they dispersed on the interface. The vertical motion of these particles during their trapping is not discussed because the present experimental setup did not allow to monitor their motion normal to the interface because of their small size.

Figure 5.8 shows the vertical motion of glass particles with diameter between 580 µm and 2 mm, and of a 1.45 mm mustard seed, and of 2.0 and 3.75 mm plastic beads. The floating height depends on the densities of the particle and the liquids, and on the contact angle. For glass particles of the same type, the floating height increased with

decreasing diameter, and the time taken to reach equilibrium decreased with decreasing diameter. The floating height on the decane-water interface of particles smaller than approximately 1 mm decreased slowly before reaching a constant value. This was not the case for the same particles on the air-water interface. It could be due to the fact that when a particle smaller than 1 mm moved downward in the decane-water interface, the three-phase contact line became partially pinned on the particle's surface increasing the contact angle above the equilibrium value. This in turn increased the vertical capillary force making the net vertical force on the particle zero even though the particle was above its equilibrium height. As the contact line slowly moved downward on the particle's surface, the contact angle was reduced and the particle moved downward.

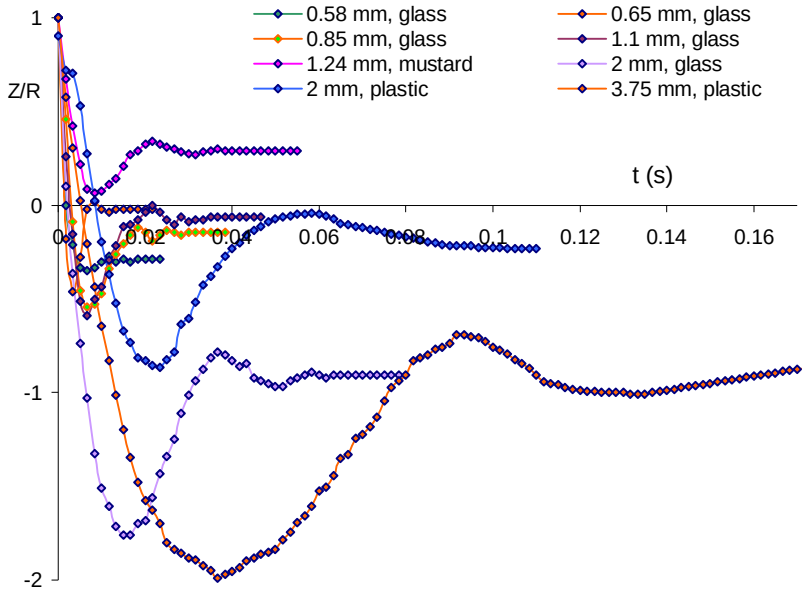

Figure 5.8(a) The dimensionless vertical positions (Z/R) as a function of time after the particles come in contact with the air-water interface.

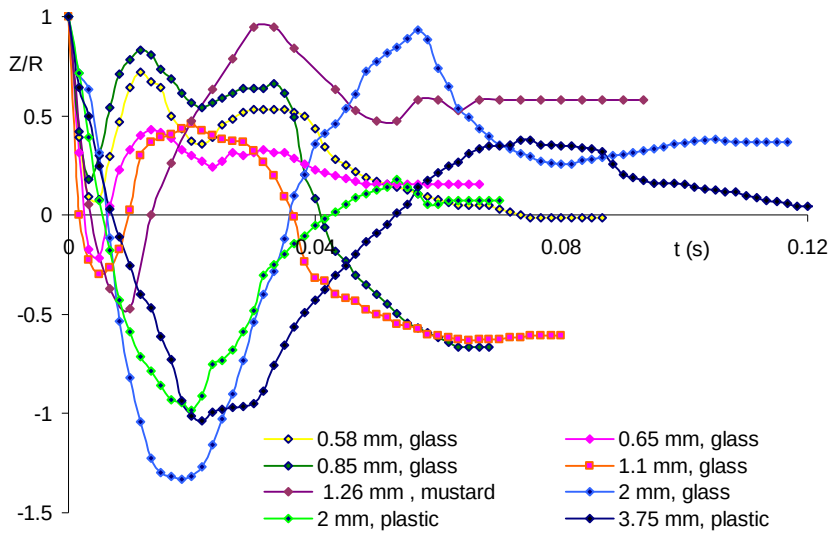

(b)

Figure 5.8(b) The dimensionless vertical positions (Z/R) as a function of time after the particles come in contact with the decane-water interface.

A comparison of the two cases described in Figure 5.8a also shows that the time taken by the particle to oscillate once about the equilibrium height, i.e., the inverse of which is the frequency of oscillation, is larger on the decane-water interface. Since the effective interfacial viscosity is larger when the upper fluid is decane and the interfacial tension and the buoyant weight of the particle for the decane-water interface are both smaller than the corresponding values for the air-water interface, the experimental result for the frequency of oscillation is consistent with the analysis according to which the frequency decreases with decreasing interfacial tension, decreasing buoyant weight and increasing viscosity.

The dependence of the frequency of oscillation of glass particles on the air-water and decane-water interfaces on their diameter was also investigated. These results are shown in Figure 5.9. For both interfaces, the frequency increased with decreasing particle

size. The frequency of oscillation was larger on the air-water interface than of the same particle on the decane-water interface. These results are in agreement with the analytical results.

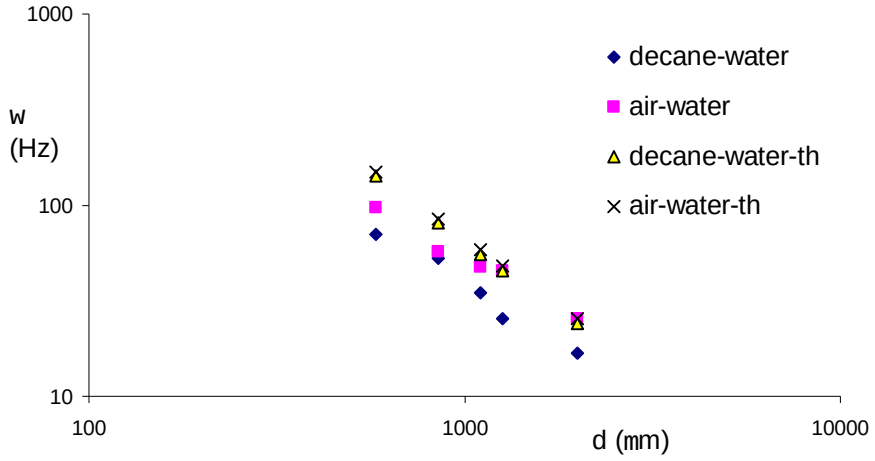

Figure 5.9 The frequency of oscillation of spherical glass particles on the decane-water and air-water interfaces versus the particle diameter. The parameter values in Eq. (7) are assumed to be: $\rho_p = 2600.0$ kg/m3 and $\rho_p - \rho_c = 1600$ kg/m3; for the air-water interface $\mu = 0.001$ Pa.s, $\gamma_{12} = 72.4$ mN/m; and for the decane-water interface $\mu = 0.001$ Pa.s, $\gamma_{12} = 51.2$ mN/m.

5.4 Flow Induced on the Interface

To investigate the fluid motion induced at the interface due to the adsorption of a test particle, the interface was seeded with 100 μm sized tracer glass particles. The tracer particles were small compared to the test particle so that they did not significantly influence the fluid motion caused by the test particle. The velocity of tracer particles decreased with increasing distance from the test particle (Figure 5.10) and also decreased with time (Figure 5.11). The total distance traveled away from the test particle depended on its initial distance from the test particle. From Figures 5.8 and 5.11 it can be noted that even after the vertical oscillations of a 580 mm particle subsided at t = ~0.03 s, tracer

particles on the interface continued to move apart for t < ~0.22 s. This shows that the flow induced at the interface by a test particle persists even after the particle attains vertical equilibrium.

The same trend for interfacial fluid velocity was observed when two identical test particles were dropped simultaneously onto the air-water interface, but the velocity was almost double that of when a single glass particle was dropped.

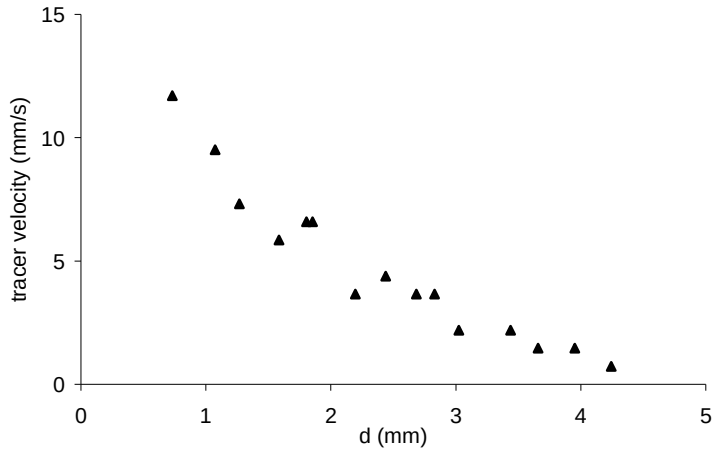

Figure 5.10 The velocity of tracer particles on the air-water interface is plotted as a function of the distance (d) from the center of a test glass particle. The velocity distribution plotted here is at a time 0.033 s after the particle was trapped at the interface. The data were taken for 3 different particles of the same approximate diameter of 550μm.

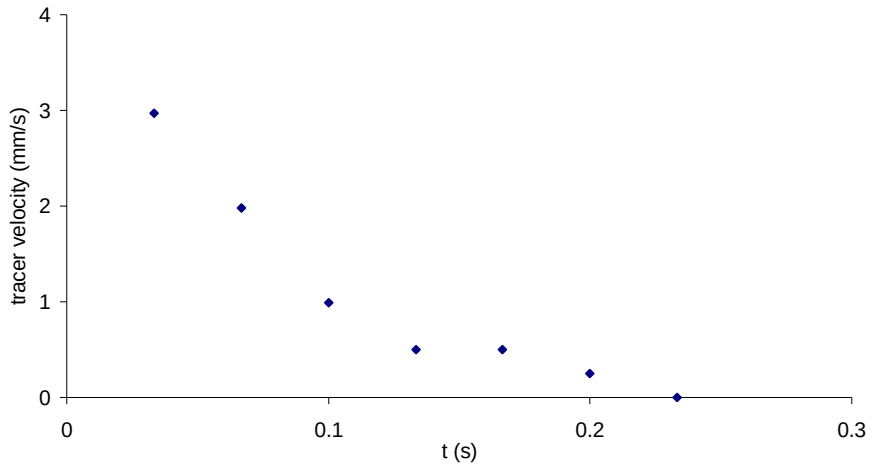

Figure 5.11 The velocity of a tracer particle on the air-water interface initially at a distance of 2.31 mm from a glass test particle of diameter 550 μm is shown as a function of time. The velocity became negligibly small at t = ~0.24 s.

5.5 Simultaneous Adsorption of Two Particles

Two particles released simultaneously and near each other above a fluid-liquid interface were trapped at the interface by the same mechanism by which a single particle was trapped. Specifically, they were pulled into the interface and oscillated vertically several times before the amplitude of oscillation became negligibly small (Figure 5.12). In addition, the particles moved apart from each other along the line joining their centers.

Figure 5.12a shows the adsorption of two mustard seeds of the same approximate size on the decane-water interface. After they touched the interface, they were pulled inwards by the vertical capillary force which was followed by vertical oscillations about their equilibrium positions. During this time they also started to move apart because of the hydrodynamic force and the interfacial flow resulting from the particles motion normal to the interface. The oscillations decayed after some time, but the particles continued to move apart because of the induced interfacial flow.

After the particles stopped moving apart, they clustered back together under the action of lateral capillarity forces which arise because of the deformation of interface caused by the particles. The behavior of two mustard seeds released onto the air-water interface, as shown in Fig.5.12b, was qualitatively similar, except that the velocity with which they moved apart and their maximum separation were larger than on the decane-

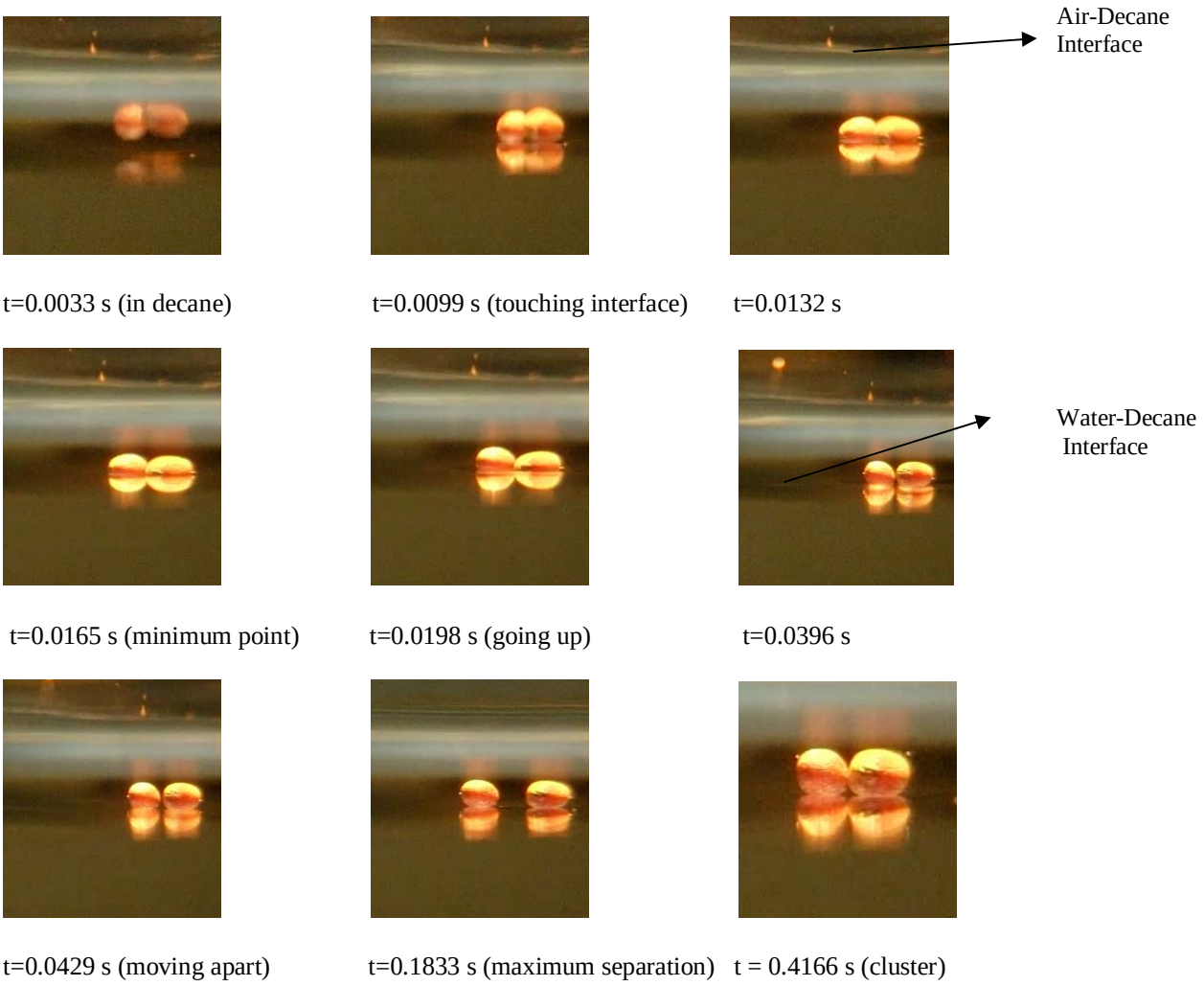

Figure 5.12 (a) A sequence of photographs showing the trapping, dispersion and clustering of two mustard seeds on decane-water interface.

t=0

t=0.0033 s (going down)

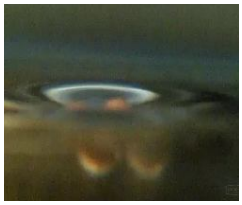

t=0.01 s (minimum height)

t=0.0166 s (going up)

t=0.02 s

t=0.0233 s (maximum height)

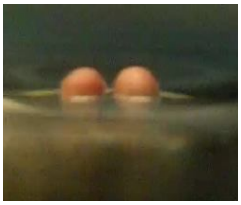

t=0.03 s (moving apart)

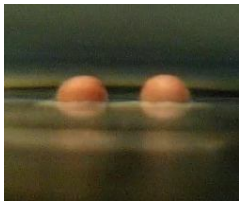

t=0.0533 s

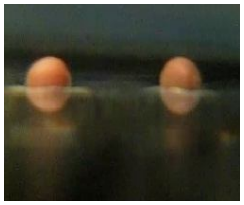

t=0.266 s (maximum separation)

t = 0.8366 s (cluster)

Figure 5.12 (b) A sequence of photographs showing the trapping, dispersion and clustering of two mustard seeds on fluid-liquid interfaces air-water interface.

water interface. It may also be noticed that in both cases although the particles started to move apart immediately after they came in contact with the interface, this became apparent only after approximately one vertical oscillation.

The gap between the particles for the above two cases is shown as a function of time in Figure 5.13. It may be noted that the particles reached their maximum lateral velocity shortly after they came in contact with the interface. The figure also shows that

the velocity with which they initially moved apart was larger than the velocity with which they later approached each other. This implies that the forces that cause the initial dispersion are stronger than the attractive lateral capillary forces that arise because of their buoyant weight.

From Figures 5.12 and 5.13, note that the time interval for which the particles oscillated vertically after coming in contact with a fluid-liquid interface was several times smaller than the time interval for which they moved apart. Thus, the interfacial flow caused by the particles persisted, and continued to move nearby particles apart, even after their vertical oscillations become indiscernible.

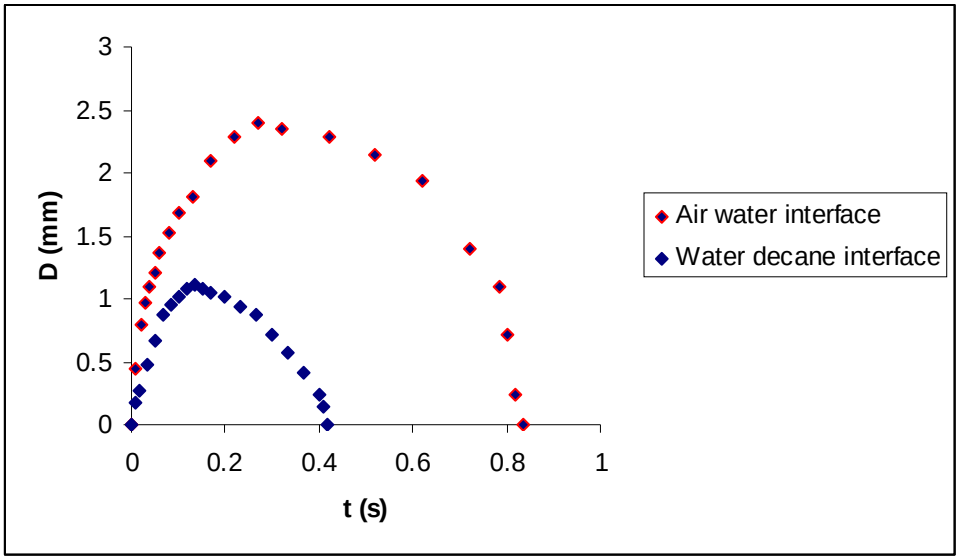

Figure 5.13 The gap (D) between two mustard seeds is shown as a function time after they came in contact with the air-water and water-decane interfaces. The diameter of mustard seeds was ~ 1.3 mm. The maximum gap and the maximum velocity were larger on the air-water interface.

5.6 Adsorption of Particle Clusters

In this section, the dispersion of small clusters of particles is described when they come in contact with the corn oil-water and decane-water interfaces. Glass particles of diameter ranging from 5 to 120 μm were used in this study. Particles were sprinkled onto the surface of the upper liquid where they were allowed to cluster, and then were pushed downward making them sediment to the liquid-liquid interface.

Figure 5.14 shows dispersion of 45 μm glass spheres on the corn oil-water interface. Notice that since the velocities with which the particles of the cluster sedimented were different, they did not reach the interface at the same approximate time, but instead over a period of time which lasted for a few seconds (also Figures 5.15-5.16). This situation is different from the case when particles are sprinkled through the air onto a liquid surface where all of the particles reach the interface within a relatively short time interval. The moment particles came in contact with the interface of corn oil and water, they dispersed radially-outward into an approximately disk-shaped region. Since particles sedimenting through the corn oil took several seconds to reach the interface, the dispersion process on the interface continued for a longer time duration than on the air-water interface. Besides, the speed with which particles dispersed was smaller than on the air-water interface because of the higher viscosity of the corn oil-water interface and also because all of the particles did not reach the interface at the same approximate time. Particles already trapped on the interface remained dispersed until additional particles continued to sediment onto the interface.

Shortly after all of the particles were captured at the interface, they started to cluster under the action of lateral capillary forces. The speed with which particles clustered was smaller than the speed which they dispersed.

Furthermore, the packing density of particles within a cluster decreased with decreasing particle size. This is because the strength of capillary forces decreases with decreasing particle size and so particles do not pack tightly leaving many void spaces within the cluster. The smaller-sized particles disperse more readily, but since their size is smaller it is difficult to observe them individually. Moreover, the smaller-sized particles took a longer period of time to reach the interface and thus the time interval over which they sedimented onto the interface was longer. It was also observed that when more particles reached the interface together, the dispersion speed and the radius of the area into which they spread were larger as each particle contributed to the outward dispersion of the cluster and hence the resulting flow on the interface was stronger.

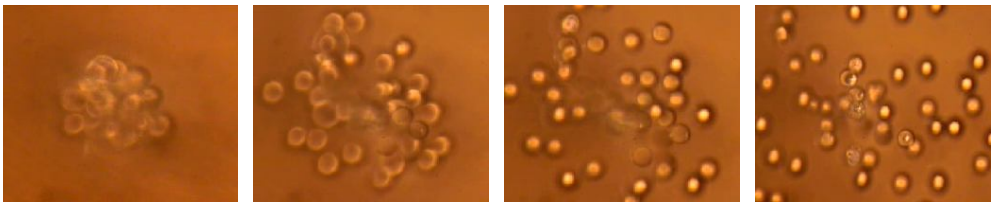

t=10 s t=12 s t=23 s t=0 s

Figure 5.14 Dispersion of 45 µm glass spheres on the corn oil-water interface. The figure shows that particles reach the interface over a time period and that they disperse violently as they come in contact with the interface. The particles trapped on the interface are in focus and those above the interface are out of focus. Initially, particles are above the interface, at t=10 s some of the particles have reached the interface, and at t= 23 s most of the particles are trapped at the interface.

Figure 5.18 shows dispersion of glass particles on the decane-water interface. As the viscosity of decane is an order of magnitude smaller than that of corn oil, particles sedimented relatively quickly and all of the particles reached the interface within a relatively shorter interval of time. As a result, the velocity with which they dispersed after coming in contact with the interface was larger. After dispersive forces subsided, particles clustered under the action of lateral capillary forces.

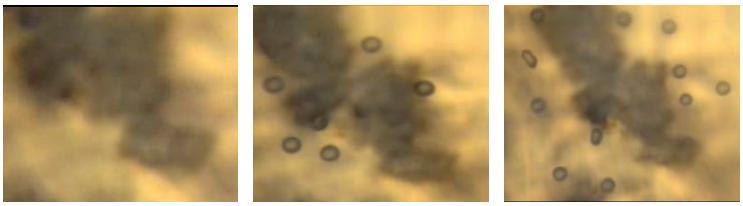

t=1 s t= 2 s t=4 s

Figure 5.15 Dispersion of 120 µm glass spheres on the corn oil-water interface. Only a few particles (those in focus) have reached the interface and dispersed. Particles continued to disperse on the interface as they came in contact with the interface.

t=0 s t= 18 s t= 24 s

t= 28 s t= 230 s t=874 s

Figure 5.16 Dispersion of 20 µm glass spheres on the corn oil-water interface. The figure shows that particles disperse as they come in contact with the interface. After all of the particles were trapped on the interface and the dispersive forces subsided, the particles clustered under the action of lateral capillary forces. The cluster is rather porous as capillary forces are relatively weaker.

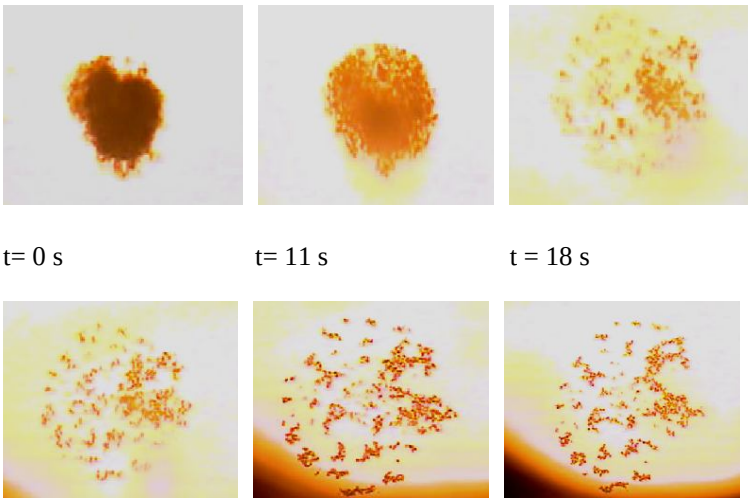

Figure 5.17 Dispersion of 5-8 µm glass spheres on the corn oil-water interface. Particles disperse as they reach the interface.

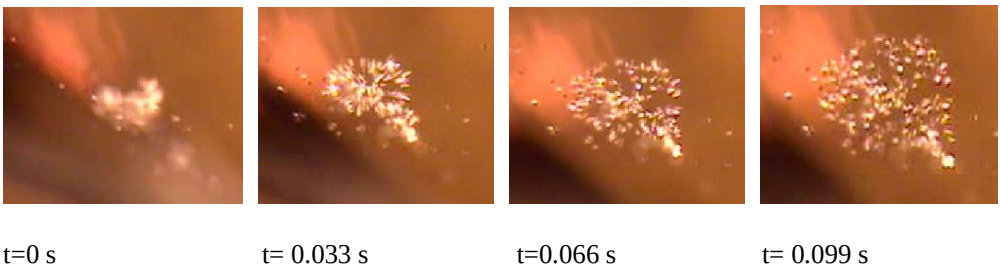

Figure 5.18 Dispersion of 45 µm glass spheres on the decane-water interface. In the first photograph most of the particles are on the decane surface, but the camera focus is on the decane-water interface which makes them out of focus. Subsequently, they became visible as they reached the decane-water interface where they were dispersed.

CHAPTER 6

BREAKUP OF PARTICLE CLUMPS ON LIQUID SURFACES

This chapter describes and explains the mechanism for the breakup of clumps of particles on liquid surfaces. Although it is known that clumps of some powdered materials breakup and disperse on liquid surfaces to form particle monolayers, the mechanism by which this happens is not entirely understood. It is shown in this chapter that a floating clump breaks up because when particles on its outer periphery come in contact with the liquid surface they are pulled into the interface by the vertical component of capillary force overcoming the cohesive forces which keep them attached and then these particles move away. In some cases, the clump itself is broken into smaller pieces and then these smaller pieces break apart by the aforementioned mechanism. The newly adsorbed particles move away from the clump, and each other, because when particles are adsorbed on a liquid surface they cause a flow on the interface away from themselves. This flow may also cause the newly exposed particles on the outer periphery of the clump to break away. Interestingly, when many particles are asymmetrically broken apart from a clump, the clump itself is pushed in the opposite direction by the flow due to the newly adsorbed particles. Since millimeter sized clumps can breakup and spread on a liquid surface within a few seconds, their behavior appears to be similar to that of some liquid drops which can spontaneously disperse on solid surfaces. However, if the capillary force is not large enough to overcome the cohesive force holding the clump together, the clump may not breakup.

When a clump of particles is placed on a liquid surface the particles near the outer periphery of the clump are broken apart first by the capillary force which pulls them into the interface. This, of course, can happen only when the capillary force is large enough to overcome the cohesive force which keeps the clump intact. The detached particles move radially outward from the clump because of the lateral interfacial flow that is induced by these newly adsorbed particles and those that are subsequently broken apart from the clump. The speed at which particles break apart is faster at first since the number of particles being broken apart per unit time is greater, and then decreases as the clump size decreases with time. The mechanism by which a clump spreads on a liquid surface is similar to that by which a pinch of powder sprinkled onto the liquid surface disperses except that for the latter the cohesive forces are negligible and so the powder disperses immediately.

6.1 Experimental Setup

In experiments, millimeter sized particle clumps were isolated and then dropped gently onto an air-liquid interface using a spatula or they were placed in an upper liquid through which they sedimented to a liquid-liquid interface. The clumps were dried for several hours in an oven to eliminate the influence of any residual moisture. Millipore water was used in this study to eliminate contaminants which can influence the interfacial properties.

The entire phenomenon of a clump breaking up into individual particles or smaller clumps and their subsequent radially outward motion on the interface away from the clump was recorded using a high-speed camera (Casio Exilim F1) and a Nikon Metallurgical MEC600 microscope (Figure 6.1). The high speed camera enabled

recording up to 1200 fps (frames per second). The high speed videos were used to study the fast transient motion of particles breaking away from the clump. The microscope which allowed for a magnification of up to 500X was used to investigate the particle scale details of the breakup. The recording speed for the microscope was 30 fps. The video recordings were later analyzed frame-by-frame to understand the mechanism for the clumps breakup.

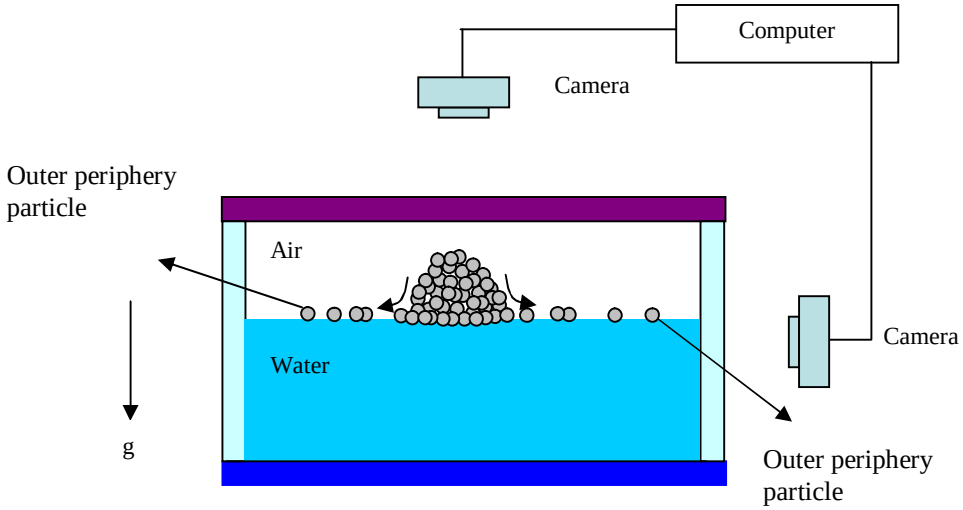

Figure 6.1 Schematic of the experimental setup used to study the spreading of a solid clump on a fluid-liquid or liquid-liquid interface.

6.2 Adsorption of a Single Particle on an Air-Liquid Interface

It was shown in [39] that when a particle comes in contact with a fluid-liquid interface the vertical component of capillary force pulls it inwards to its equilibrium position within the interface. The motion of the particle during adsorption is inertia dominated, and so it overshoots the equilibrium height (Figure 6.2). This is normally the case for micron and large sized particles on the surface of mobile liquids like water. For example, Figure 5.4 shows the adsorption of 2 mm plastic bead dropped gently on a water surface

in a Petri dish. The bead traveled downward below its equilibrium height and then reversed direction under the action of the capillary force. Although the viscous drag causes the particle to slow down, its magnitude is not large enough to stop the particle completely and consequently the momentum of the particle carries it below the equilibrium height. Notice that when the particle moves below its equilibrium height, the capillary force reverses its direction and acts in the same direction as the drag. Hence, after moving down some additional distance, the particle reverses its direction, leading to several oscillations and interfacial waves before the particle comes to rest. This behavior of the particle is similar to that of underdamped mass-spring-dashpot systems.

The balance among the particle's buoyant weight, the vertical capillary force, and any other vertical force acting on the particles determines its equilibrium position in the interface. The capillary force acts to bring the particle to its equilibrium position, but when the capillary force is not large enough to overcome these forces acting vertically the particle is not trapped in the interface. This is normally the case for millimeter- and larger-sized particles that are heavier than the liquid below. Micron- and nano-sized particles, on the other hand, for which the buoyant weight is negligible compared to the capillary force, are readily trapped at the interface. Furthermore, the vertical capillary and pressure forces must also overcome the momentum of the particle, which it possesses before coming in contact with the liquid surface. Owing to the fact that the capillary force acting on a particle varies linearly with the particle size, and the buoyant weight and the momentum vary as the third power of the particle radius, smaller particles are more readily captured at the interface.

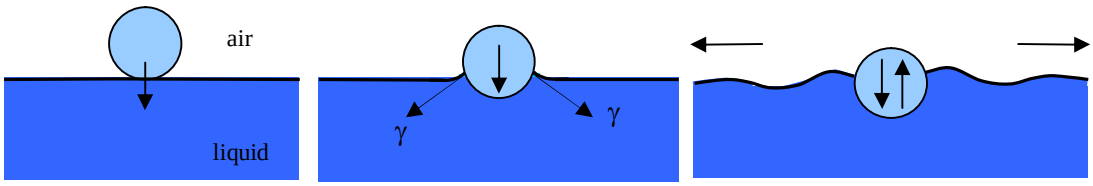

Figure 6.2 Adsorption of a particle at an interface. (First two pictures) When the particle comes in contact with the interface it is pulled inwards by the interfacial force. The particle oscillates about the equilibrium height within the interface before these oscillations induce a flow on the interface that causes small tracer particles to move away. Our experiments show that tracer particles remain trapped at the interface and move away from the test particle with a velocity which is an order of magnitude smaller that the test particle's maximum velocity normal to the interface.

It was shown in [39] that particles dropped onto a liquid surface disperse initially due to the fact that when a particle comes in contact with the surface the vertical capillary force pulls it into the interface causing it to accelerate to a relatively large velocity normal to the interface. The maximum velocity increases with decreasing particle size; for nanometer-sized particles, e.g., viruses and proteins, the velocity on an air-water interface can be as large as ~47 m/s. The vertical motion of the particle gives rise to a lateral flow on the interface away from the particle. The lateral flow was measured in [39] for particles ranging in size from a few micrometers to a few millimeters. The magnitude of flow on the interface decreased with increasing distance from the particle and decayed to zero shortly after the particle was adsorbed. Furthermore, it was also shown in [39] that the lateral flow velocity in both experiments and direct numerical simulations increased with the number of particles simultaneously adsorbed at the interface.

6.3 Breakup of particle clumps on fluid-liquid surfaces

To understand the mechanism by which clumps of particles break up on liquid surfaces, clumps were gently placed on placid liquid surfaces and recorded their breaking up using

a high-speed camera and a microscope, as shown in Figure 2. The focus of this work is to study the clumps of materials that break up when they are placed on a liquid surface, and not those that remain intact on liquid surfaces. The contact angle of the particles of a clump with the fluids involved and the cohesive force among the particles which must be overcome by the capillary force appear to be the two key factors in determining whether or not the clump breaks up. For example, clumps of Teflon powder on water remained intact for several hours, the time duration for which they were monitored, as it is hydrophobic and the cohesive forces are relatively larger.

The breaking up of the clumps of different materials including glass, carbon, nano-sized aluminum oxide, nano-sized calcium phosphate particles was studied on a water surface, and those of glass particles were studied for different particle sizes and on both air-water and corn oil-water interfaces. In the study, the size of particles used to form the clumps as well as the size of the clumps was varied which was between approximately 1-5 mm. For most cases, the moment the clump came in contact with the interface it started to lose particles from the periphery and g progressed towards the center. Eventually, the entire clump was dispersed. The clumps of silicon dioxide and titanium oxide particles were only partially captured on a water surface in the sense that after coming in contact with the water surface some of their particles were broken away from the clump and captured on the interface, but a large part of the clump sedimented to the bottom of the Petri dish.

It is noteworthy that clumps containing ~ 10-30 particles can breakup almost instantly when they come in contact with an air-liquid or liquid-liquid interface. Figure 4 shows the breakup of a small clump of 4 μm glass particles on the corn oil-water

interface. Notice that the clump (agglomerate) remained intact on the upper liquid, but the moment it came in contact with the interface the forces causing dispersion caused it to break apart. The clump broke up because it was pulled into the interface by the vertical capillary force accelerating it to a relatively-large velocity in the direction normal to the interface. The resulting viscous and shearing forces that act on the clump can overcame the weak cohesive forces holding the clump particles together. Larger clumps, on the other hand, do not break apart immediately, but start to lose particles from their outer periphery as described above.

t=0 s t=0.033 s

Figure 6.3. Breakup and dispersion of an agglomerate of glass spheres on the interface of corn oil and water, looking down from above (500x mag.). The size of glass particles was ~4 μm. (left) An agglomerate sedimented through corn oil and was captured at the interface. (right) After coming in contact with the interface it breaks apart explosively dispersing radially-outward into an approximately circular region. Notice that some of the particles remained agglomerated.

The behavior of two different clumps of the same material varied as the cohesive forces for them vary. For example, sometimes the broken pieces were not individual particles but smaller clumps or even into two or more clumps of comparable sizes because of the structural faults in the clump. These smaller clumps broke up subsequently by the aforementioned mechanism. However, some of the very small clumps of approximately 2-5 particles remained intact for several minutes and some did not breakup completely for several minutes. This perhaps was due to the fact that the cohesive forces

for these small clumps (agglomerate) were relatively larger. Their behavior could not be monitored for longer time durations as particles started to cluster under lateral capillary forces [15, 16, 40].

6.4 Breakup on Air-Water Interface

Figure 6.5 shows the breakup of a clump of glass particles (Soda-lime-borosilicate glass Bubbles, 3M Scotchlite Glass) and of corn starch on a water surface. The clumps were dropped from a height of approximately 2 mm onto the water surface in a Petri dish. In both cases, as soon as the clumps touched the water surface, the particles on the outer periphery of the bottom portion of the clump started to race radially outward from the clumps which made the clump lose mass with time. As a result, the height of the clump decreased with time. The clump of glass particles shown in Figure 6.5a broke up completely into a monolayer on the water surface after 7.2 s. The clump of corn starch shown in Figure 6.5b, on the other hand, broke up in about 0.3 s. The speed with which the corn starch particles moved away from the clump was also larger. In both cases, a significant fraction of the particles up to 10-20% were not trapped on the air-water interface. These particles slowly settled to the bottom of the Petri dish.

Figure 6.6a shows the breakup of a clump of glass particles obtained using a camera mounted above the water surface. The same particles were used in Figure 6.5a. The figure shows that the clump started to lose particles from the outer periphery before breaking into smaller clumps. These smaller clumps along with the main clump subsequently broke up to form a monolayer of particles on the water surface. The phenomenon took about 13.8 s to complete. This time is slightly smaller than the time in Figure 6.5a where the clump size was smaller.

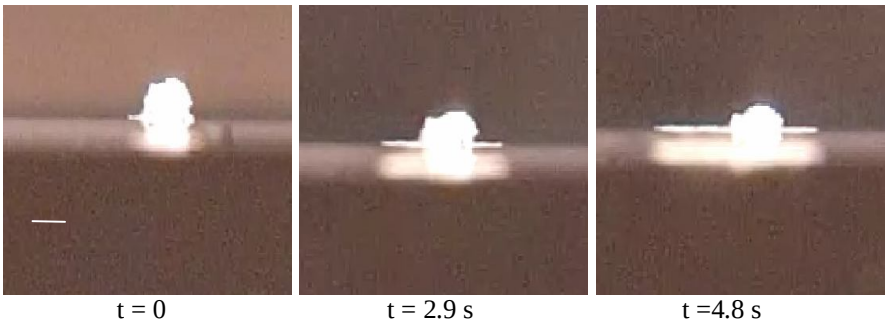

(a)

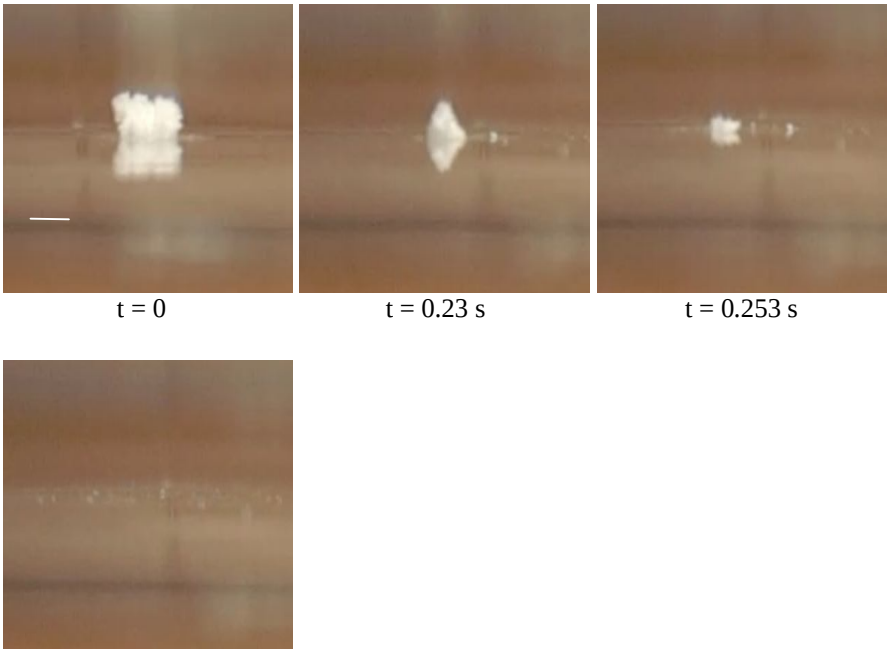

(b)

Figure 6.4. A sequence of photographs showing a side view of the breakup of the clumps of particles on an air-water interface. The first photographs show the clumps shortly after they came in contact with the water surface and the final photographs show the monolayer of particles formed because of their breakup. The photographs were taken at 300 fps. (a) A 1.3 mm clump of 10-170 μm glass particles (scale bar = 1 mm); (b) a 1.6 mm clump of corn starch. The size of particles is 28-160 μm (scale bar = 1 mm).

The time in which the clumps of approximately equal sizes broke apart was of the same order, but varied slightly. This variation is expected since the compositions of clumps vary. The time in which the clumps broke up in our experiments increased with increasing clump size.

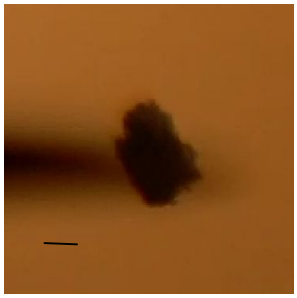
t = 0 s


t = 0.003 s

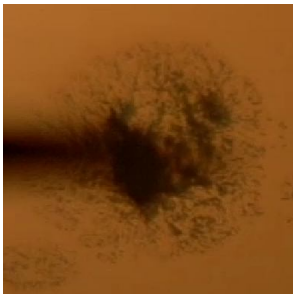
t = 0.03 s

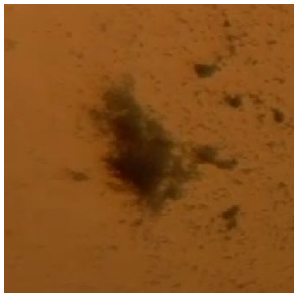
t = 0.2 s


t =8.8 s

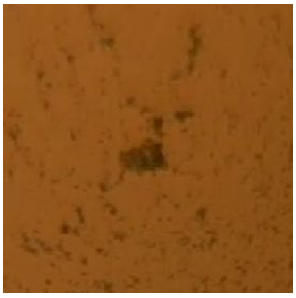
t =12.5

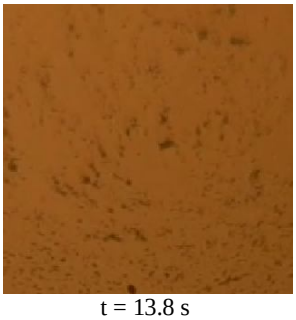
t = 13.8 s

(a)

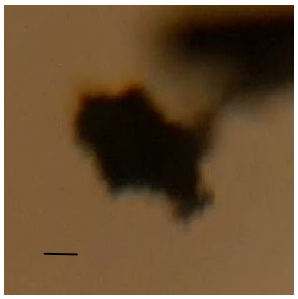

t = 0

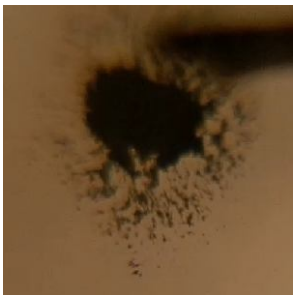

t = 0.034 s

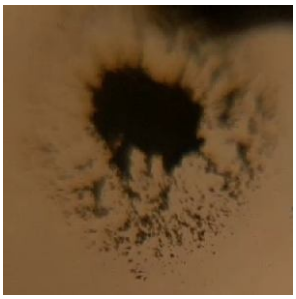

t = 0.067 s

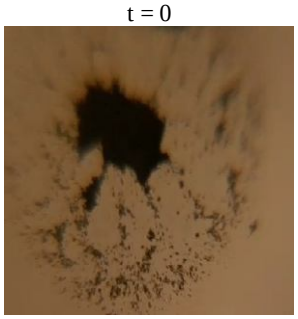

t = 0.134 s

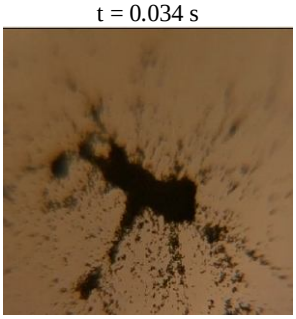

t = 1.67 s

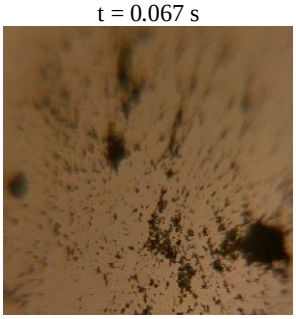

t = 4.0 s

t = 11.34 s

(b)

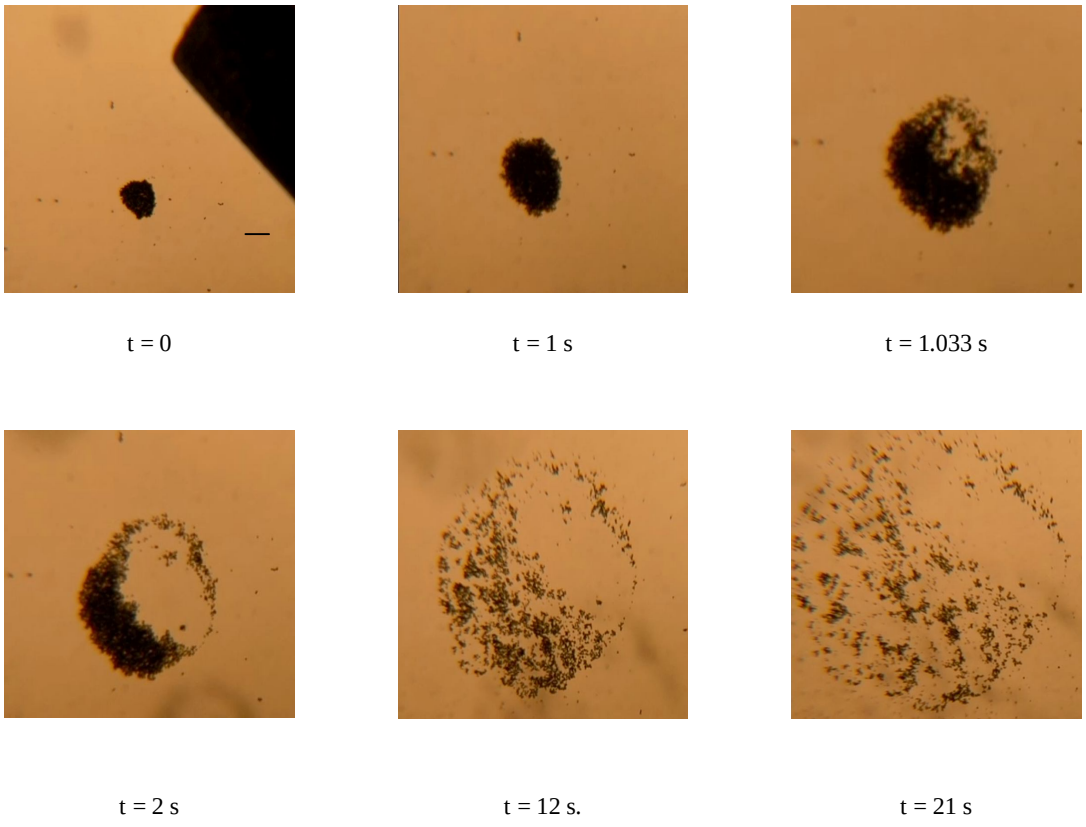

(c)

Figure 6.5 A sequence of photographs taken using a camera mounted above showing the breakup of the clumps of glass and carbon particles on an air-water interface. The clump loses particles from all of the sides, but not uniformly. The photographs were taken at 300 fps. After the clump breaks up completely, its particles form a monolayer on the water surface. (a) A 3.66 mm clump of 10-170 μm glass particles; (b) A 4.92 mm clump of 12-50 μm glass particles. (c) A 1.54 mm clump of 65-110 μm carbon particles. Scale bar = 1 mm.

Figure 6.5b shows the breakup of a clump of 12-50 μm hollow glass particles (Potters Q-CEL 300 - Sodium Silicate, Sodium Borate) and Figure 6.5 (c) of a clump of 65-110 μm carbon particles on an air-water interface. Again, the moment the clumps touched the water surface the particles on its outer periphery of the clump raced to move away radially, overcoming the cohesive forces. Notice that in addition to individual particles some of the broken pieces were smaller clumps. These smaller clumps subsequently broke up by the same mechanism. The clump of 12-50 μm hollow glass particles was broke up into a monolayer in 11.34 s. Also, even though the initial clump

size was larger, the time taken to breakup was smaller than in Figure 6.5 (a). This is due to the fact that the average size of particles in Figure 6.5 (b) is larger and the clumps of smaller particles break apart more quickly.

To understand the mechanism at particle scales by which clumps break up, a magnification of 25X was used to observe individual particles. The size of the clump used in this study was ~ 1mm to ensure that the entire clump was visible under the microscope (Figure 6.6 (a)). The breakup mechanism was similar to that for the millimeter size clumps of Figure 6.6, except that it broke up relatively faster. Also, since the speed of recording for the microscope was only 30 fps, the rapid motion of the particles caused streak lines to form which was in fact helpful in interpreting their trajectories. This did not happen in Figure 6.6 for which the recording speed was ten times larger. Notice that the clump broke up into smaller clumps and then these smaller clumps broke up by losing particles from their periphery. After their breakup from the clump, particles moved away from each other (Figure 6.6 (b)). The average separation between particles was around two times the diameter. Some of the smaller clumps, however, did not break up completely. This perhaps was due to the fact that the cohesive force keeping them intact were too strong to be overcome by the capillary force.

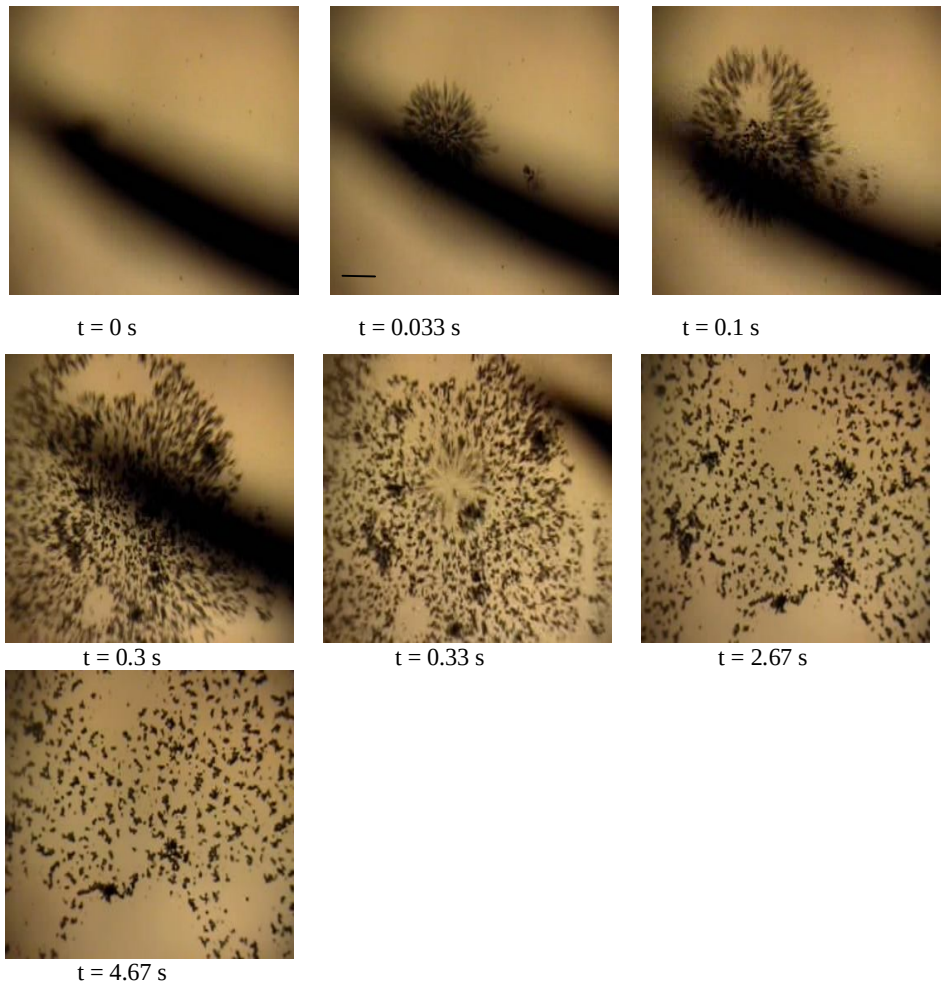

(a)

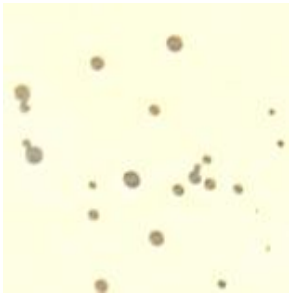

(b)

Figure 6.6 A sequence of photographs showing the breakup of a small clump of 10-170 μm glass particles on an air-water interface. The photographs were taken at 30 fps and a magnification of 25X. (a) The clump initially breaks up and its particles disperse radially outward relatively violently. The streak lines form because the recording speed is only 30 fps. The small clusters which broke away from the primary clump also broke up with time. The spatula used to drop the clump is also visible in the first four photographs. Scale bar = 0.5 mm. (b) The picture shows that particles are away from each other soon after they disperse breaking from the clump. The photographs were taken at 30 fps and a magnification of 200X.

Another interesting feature of the breakup was that the ejection of particles in a direction from the clump propelled the clump in the opposite direction. The first photograph in Figure 6.7 shows a clump of 10-170 µm glass particles just after it was placed on the air-water interface. The second photograph in the sequence shows the ejection of particles at high speeds from the upper surface of the clump. This, as the third photograph shows, causes the clump to move in the downward direction. The clump stopped moving when particles were ejected more uniformly from its periphery or the ejection of particles stopped.

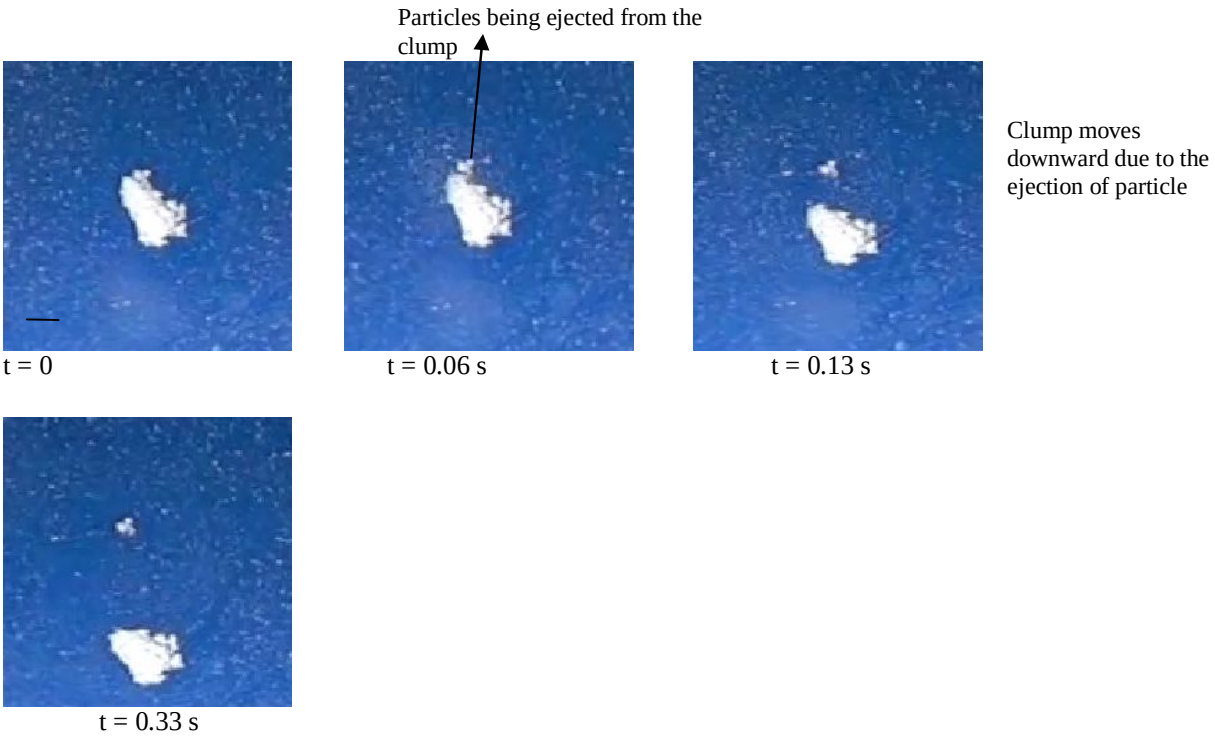

Figure 6.7. A sequence of photographs showing the motion of a clump of 10-170 µm glass particles on an air-water interface due to the non uniform ejection of particles. The second photograph shows that the ejection of particles from the upper surface of the clump. The clump experiences a thrust in the downward direction which causes it to move in the downward direction. The clump stopped moving after particles were ejected uniformly from all sides. Scale bar = 1 mm.

6.5 Breakup on Corn Oil-Water Interface

The breakup of a clump of glass particles on a corn oil-water interface is described next. Experiments were conducted in a Petri dish which was filled with water at the bottom and corn oil on the top. A millimeter size clump was dropped on the corn oil surface. The clump settled without breaking through the corn oil to the corn oil–water interface. The microscope was used to record its breakup at the interface. The recording speed was 30 fps and the magnification 25X.

Figure 6.8 shows that the moment the clump came in contact with the interface particles from its outer periphery started moving radially outward violently, as was the case on an air-water interface. The clump broke into smaller pieces before disintegrating completely. These smaller clumps continued to lose particles and completely broke up into a monolayer at 25 s.

However, some of the smaller pieces of the clump did not remain trapped at the interface and sedimented to the bottom to the Petri dish. This perhaps is due the fact that the interfacial tension of 33.2 mN/m for the corn oil-water interface is smaller than that of an air-water interface. Also, the speed with which particles dispersed on the corn oil-water interface was slower than on an air-water interface and the time taken by the clumps to breakup was larger than on an air-water interface. For example, a 3.66 mm clump broke up in 13.8 s on an air-water interface, and a 1.86 mm clump, even though smaller, took 25 s to break up on a corn oil-water interface. The motion of particles on the corn-oil water interface is slower because its effective fluid viscosity is larger than of the air-water interface.

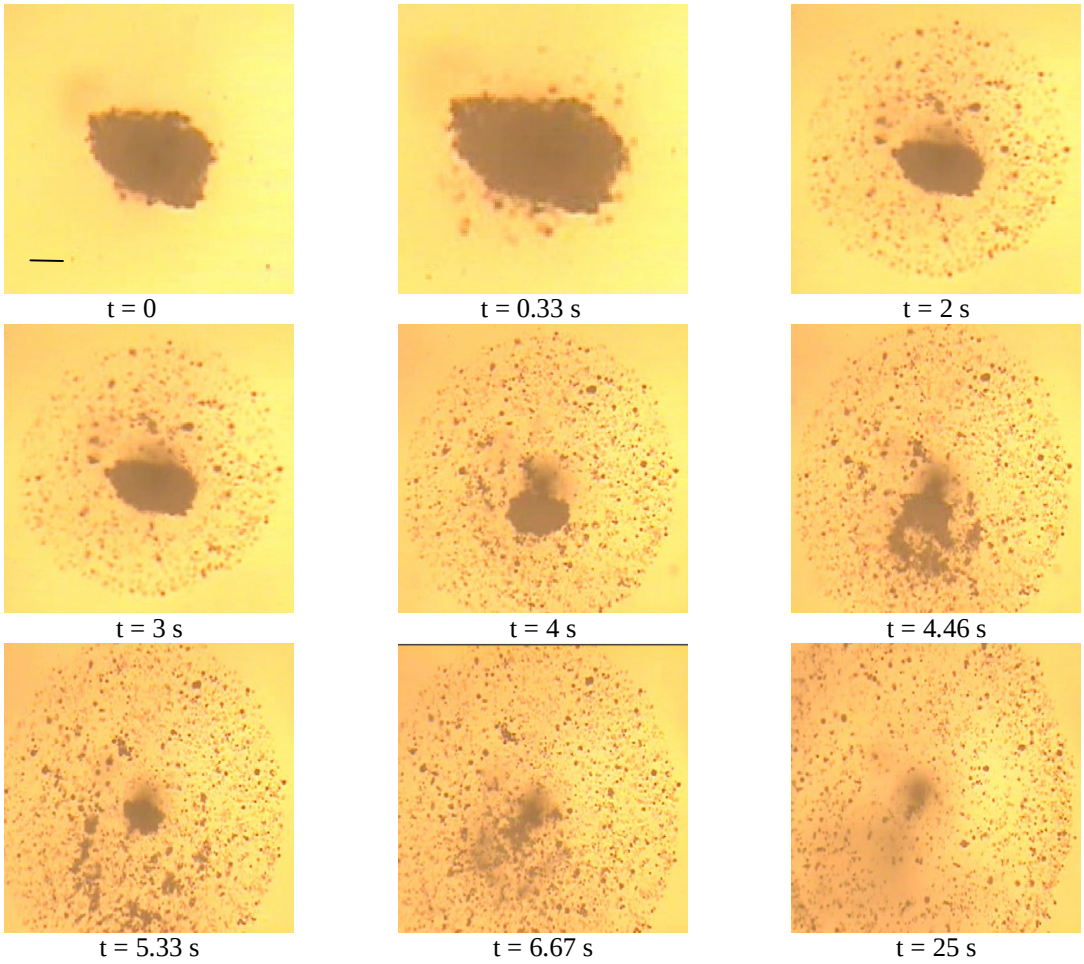

Figure 6.8. A sequence of photographs showing the breakup a clump of 10-170 µm glass particles on the corn oil-water interface. The size of the clump is around 1.86 mm. The clump dropped on the corn oil surface settled through it to reach the corn oil-water interface and dispersed violently at the interface. The clump loses particles from all of the sides, and breaks into smaller clumps before breaking up completely to form a monolayer on the interface. The photographs were taken at 30 fps. Scale bar = 0.5 mm.

CHAPTER 7

CONCLUSIONS

It is shown that when a particle comes in contact with a liquid surface it is pulled into the interface towards its equilibrium height by the vertical capillary force and that during this process the particle can accelerate to a relatively large velocity normal to the interface. For example, a particle of radius 100 μm sprinkled onto the water surface may attain a velocity of the order of 1 m/s. The maximum velocity on an air-water interface, which increases with decreasing particle size, can be as large as ~47 m/s. It is also shown that a particle being adsorbed oscillates about its equilibrium height before coming to rest under viscous drag. These oscillations of the particle cause the fluid around it to move away which in our experiments was measured using smaller tracer particles that were present on the liquid surface.

When two or more particles are dropped simultaneously onto the surface their motion in the direction normal to the interface (and to the line joining their centers) gives rise to the strong repulsive hydrodynamic forces which cause them to move apart. The velocity with which particles move apart increases with increasing number of particles. Also, smaller sized particles disperse more readily because the importance of interfacial forces increases with decreasing particle radius. An analysis of the particle's equation for the vertical motion is used to determine the dependence of the velocity on the factors such as the fluid viscosity, the change in the interfacial energy due to the adsorption of the particle, the particle radius and the buoyant weight. The viscous drag causes the oscillatory motion of particles about their equilibrium heights to decay with time, and thus the repulsive hydrodynamic forces that arise because of this motion also decrease

with time. As a result, after reaching a maximum value, the velocity with which particles move apart decreases with time. Furthermore, if the buoyant weight of particles is not negligible, e.g., 200 μm sized sand particles used in Figure 1, they also experience attractive lateral capillary forces that arise because of the deformation of the interface. Although these attractive lateral forces are relatively weaker, after the repulsive hydrodynamic forces become smaller they cause particles to come back to cluster. The velocity with which particles come back to cluster however is much smaller. Micron and nano sized particles, on the other hand, remain dispersed since for them the attractive capillary forces are negligible.

Experiments also show that when particles come in contact with a liquid-liquid interface they spontaneously disperse as they do on the air-liquid interface. Specifically, experiments were conducted in which glass and other particles with diameter ranging from 5 μm to 4 mm were sprinkled onto a liquid-liquid interface. The upper liquid in these studies was decane or corn oil and the lower liquid was water. Particles sedimented through the upper liquid onto the interface where they dispersed while remaining trapped at the interface. All of the particles mentioned above were captured and dispersed on the decane-water interface. However, on the corn oil-water interface, only glass particles smaller than ~650 μm dispersed; larger glass and plastic particles and mustard seeds did not disperse. In fact, a significant fraction of these latter particles was not even captured at the interface. This perhaps is due to a smaller interfacial tension of the corn oil-water interface.

When the upper fluid was a liquid, and not a gas, particles sedimented to the interface slowly due to the higher viscosity of the upper liquid, and did not reach the

interface around the same approximate time. Since particles reached the interface over an interval of time, the dispersion occurred over a longer time interval and was relatively weaker than for the case when the upper fluid was a gas. The rate of dispersion on the corn oil-water interface was weaker than on the decane-water interface as the corn oil viscosity is smaller than the decane viscosity.

The frequency of vertical oscillation of a particle increased with decreasing particle size on both air-liquid and liquid-liquid interfaces. The frequency on the decane-water interface was slightly smaller than on the air-water interface. For a ~500 μm particle the frequency on the decane-water interface was around 100 Hz. The results for the frequency of particles between 500 μm and 3.0 mm diameter were in agreement with our analytical result for the frequency given by Eq. 4.17. Our experimental technique did not allow us to measure the frequency of particles that were smaller than ~500 μm. This agreement is noteworthy since the only parameters contained in Eq. 4.17 are the properties of the fluids and the particle, i.e., it contains no adjustable parameters.

Experiments have also shown that for small particles the partial pinning of the contact line on the particle's surface is important. When this happened the particle did not oscillate vertically about its equilibrium floating height, but instead about a height that was higher while continuing to slowly move downward in the interface as the contact line receded downward on its surface. The pinning of the contact line occurred only when the particle size was small, and since our present experimental setup did not allow us to study the motion of particles smaller than ~500 μm in the normal direction to the interface, this issue will be investigated in a future study.

After the forces causing dispersion subsided, particles clustered under the action of lateral capillary forces. For the two-particle case, the time taken to cluster was about three times larger than the time taken by them to move apart and the maximum velocity for the latter was about six times larger, indicating that the forces causing dispersion are stronger than those causing clustering. Similarly, a cluster of particles dispersed with a relatively-larger speed than the speed with which its particles clustered.

The experiment was conducted to study the mechanism by which clumps of particles loosely held together by weak cohesive forces break up when they come in contact with a fluid-liquid interface. It is shown that when a clump comes in contact with a liquid surface the particles located at its outer periphery are pulled into the interface by the capillary force overcoming the cohesive forces which keep them attached with the clump. The clump continues to lose particles from its outer periphery progressing towards the center. The detached particles move radially outward from the clump because of the lateral interfacial flow that is induced by the newly adsorbed particles and those that are subsequently broken apart from the clump. The speed at which particles break apart is faster at first since the number of particles being broken apart per unit time is greater, and then decreases as the clump size decreases with time. In some cases, the clump itself is broken into smaller pieces and then these smaller pieces break apart by the aforementioned mechanism. Also, clumps containing approximately 10-30 particles can break up almost instantly when they come in contact with a liquid surface.

The newly adsorbed particles move away from the clump, and each other, because when particles are adsorbed on a liquid surface they cause a flow on the interface away from themselves. Consequently, the initial distance between particles of the monolayer

formed due to the breakup of a clump is several times the particle diameter. After the flow due to the particles adsorption subsides, they cluster under the action of lateral capillary forces to form monloayers in which particles touch each other. The clumps used in this study contained particles of size 4 to 170 μm, and the clump size was between 1 to 5 mm.

The flow induced on the interface may also cause additional particles to detach from the clump. The important role that the flow on the interface plays can be seen when many particles asymmetrically break from the clump. In this case the clump moves in the opposite direction of that in which the newly detached particles moved away from the clump. This process of particles breaking away from the clump continues until all the particles break away to form a monolayer of particles on the liquid surface.

A millimeter sized clump can break up and spread on a liquid surface in a few seconds and thus it appears that clumps of some materials can spontaneously spread on a liquid surface, just like some drops can spread on some solid surfaces. The mechanism by which a clump spreads on a liquid surface is similar to that by which a pinch of powder sprinkled onto the liquid surface disperses except that for the latter the cohesive forces are negligible and so the powder disperses immediately. More specifically, in the latter case, since the particles are not attached to each other, they all come in contact with the liquid surface at almost the same time and so disperse explosively. In the former case, not all of the particles come in direct contact immediately with the liquid surface. Thus, only those particles that come in contact with the liquid surface are broken away from the clump and disperse, and also only when the capillary force is large enough to overcome the cohesive force holding particles together. The process continues as the new layers of

particles come in contact with the interface. Consequently, a clump spreads on a liquid surface relatively slowly.

References

1.Murray, C. B., Kagan, C. R., & Bawendi, M.G. (2000). Synthesis and characterization of monodisperse nanocrystals and close-packed nanocrystal assemblies. Annu. Rev. Mater. Sci. 30, 545–610.

2.Tan, Z., Zhang, Wang, Y., Glotzer, S. C., & Kotov, N. A. (2006). Self-assembly of CdTe nanocrystals into free-floating sheets. Science, 314, 274–278.

3.Bowden, N. A., Terfort, A., Carbeck, J., & Whitesides, G. M. (1997). Self-assembly of mesoscale objects into ordered two-dimensional arrays. Science, 276, 233–235.

4.Grzybowski, B. A., Bowden, N., Arias, F., Yang, H., & Whitesides, G. M. (2001). Modeling of menisci and capillary forces from the millimeter to the micrometer size range. J. Phys. Chem. B, 105, 404–412.

5.Wasielewski, M. R. (1992). Photoinduced electron transfer in supramolecular systems for artificial photosynthesis. Chem. Rev. 92, 435.

6.Balzani, V., Venturi, M., & Credi, A. (2003). Molecular Devices and Machines. Wiley VCH, Weinheim.

7.Aubry, N., Singh, P., Janjua M., & Nudurupati, S. (2008). Assembly of defect-free particle monolayers with dynamically adjustable lattice spacing, Proceedings of the National Academy of Sciences 105, 3711-3714.

8.Aveyard, R. & Clint, J.H. , (1996) J. Chem. Soc., Faraday Trans., 92, 85-89.

9.Binks, B.P. (2002) Current opinion in Colloid and Interface Science, 7, 21-41.

10.Chan DYC, Henry JD, Jr, White LR (1981) The interaction of colloidal particles collected at the fluid interface, J Colloid Interf Sci 79:410–418.

11.Gifford, W. A., & Scriven, L. E. (1971). On the attraction of floating particles. Chem. Engr. Sci. 26, 287-297.

12.Fortes MA (1982) Attraction and repulsion of floating particles. Can J Chem 60:2889–2895.

13.Katoh K, Fujita H, Imazu E (1992) Motion of a particle floating on a liquid meniscus surface. J Fluids Engrg 114:411–417.

14.Kralchevsky, P.A. Paunov, V.N. Ivanov, I.B. & K. Nagayama, (1992) J. Colloid Interface Sci., 151, 79 -94.

15.Nicolson MM (1949) The interaction between floating particles. Proc Camb Philos Soc 45:288–295.

16.Singh, P., and Joseph, D. D. (2005). Fluid dynamics of floating particles. J. Fluid Mech., 530, 31–80.

17.Cox PA, Knox RB (1989) Two-dimensional pollination in hydrophilous plants: Convergent evolution in the genera Halodule (Cymodoceaceae), Halophila (Hydrocharitaceae), Ruppia (Ruppiaceae), and Lepilaena (Zannichelliaceae). Amer J Bot 76:164–175.

18. Cox PA (1988) Hydrophilous pollination. Annu Rev Ecol Syst 19:261–280.

19. Short FT, Wyllie-Eciieverria S (1996) Natural and human-induced disturbance of sea grasses. Environ Conserv 23:17–27.

20. Hughes AR, Williams SL, Duarte CM, Heck KL, Jr, Waycott M (2009) Associations of concern: Declining seagrasses and threatened dependent species. Front Ecol Environ 7:242–246.

21.Bresme, F. & Oettel, M. (2007). J. Plys.: Condens. Matter, 19, 413101.

22.Lehle, H. & Oettel, M. (2007). Physical Rev. E, 75, 011602.

23.Stamou, D. & Duschl, C. (2000). Physical Rev. E, 62, 5263-5272.

24 O. Planinsek, et al., The utilization of surface free-energy parameters for the selection of a suitable binder in fluidized bed granulation, International Journal of Pharmaceutics. 207 (1–2) (2000) 77–88.

25 Z. Tuske, et al., The role of the surface free energy in the selection of a suitable excipient in the course of a wet-granulation method, Powder Technology. 155 (2) (2005) 139–144.

26 Z.G. Buckton, The use of surface energy values to predict optimum binder selection for granulations, International Journal of Pharmaceutics. 59 (2) (1990) 155–164.

27 L. Galet, et al., The wetting behaviour and dispersion rate of cocoa powder in water, Food and Bioproducts Processing. 82 (4) (2004) 298–303.

[28]N. Eshtiaghi, et al., Liquid marble formation: spreading coefficients or kinetic energy? Powder Technology. 196 (2) (2009) 126–132.

[29]K.P. Hapgood, B. Khanmohammadi, Granulation of hydrophobic powders, Powder Technology 189 (2009) 253–262 (special issue on granulation).

[30] R.C. Rowe, Surface free energy and polarity effects in the granulation of a model system, International Journal of Pharmaceutics. 53 (1) (1989) 75–78.

[31] He, X., Barone, M.R., Marsac, P.J., Sperry, D.C., Development of a rapidly dispersing tablet of a poorly wettable compound-formulation DOE and mechanistic study of effect of formulation excipients on wetting of celecoxib, International Journal of Pharmaceutics. 353 (1–2) (2008) 176–186.

[32] Nguyen, T.H., N. Eshtiaghi, K.P. Hapgood, W. Shen, An analysis of the thermodynamic conditions for solid powder particles spreading over liquid surface, Powder Technology. 201 (2010) 306–310.

[33] M.M. Nicolson, Proc. Cambridge Philos. Soc. 45, 288(1949).

[34] Osher S, Sethian JA (1988) Fronts propagating with curvature-dependent speed: Algorithms based on Hamilton-Jacobi formulations, J Comput Phys 83:12–49.

[35] Pillapakkam SB, Singh P (2001) A Level Set Method for computing solutions to viscoelastic two-phase flow. J Comput Phys 174:552–578.

[36] Singh P, Hesla TI, Joseph DD (2003) A Modified Distributed Lagrange Multiplier/ Fictitious Domain Method for Particulate Flows with Collisions. Int J Multiphas Flow 29:495–509.

[37] Singh P, Joseph DD, Hesla TI, Glowinski R , Pan TW(2000) Adistributed Lagrangemultiplier/fictitious domain method for viscoelastic particulate flows. J Non-Newtonian Fluid 91:165-188

[38] BinderWH(2005) Supramolecular assembly of nanoparticles at liquid-liquid interfaces.Angew Chem Int Ed 44:5172–5175.

[39] Singh, P., Joseph, D.D., Gurupatham, S.K., Dalal, B. & Nudurupati, S. (2009). Spontaneous dispersion of particles sprinkled onto a liquid surface, Proceedings of the National Academy of Sciences. 106, 19761-19764.

[40] P. Singh, D.D. Joseph, I. Fischer and B. Dalal, The role of particle inertia in adsorption at fluid-liquid interfaces, to appear in Physical Review E (2011).